© 2017. Published by The Company of Biologists Ltd | Development (2017) 144, 3932-3945 doi:10.1242/dev.152199

STEM CELLS AND REGENERATION

RESEARCH ARTICLE

The splicing co-factor Barricade/Tat-SF1 is required for cell cycle and lineage progression in *Drosophila* neural stem cells

Monika K. Abramczuk[1], Thomas R. Burkard[1,2], Vivien Rolland[1,*], Victoria Steinmann[1], Peter Duchek[1], Yanrui Jiang[3,‡], Sebastian Wissel[1], Heinrich Reichert[3] and Juergen A. Knoblich[1,§]

ABSTRACT

Stem cells need to balance self-renewal and differentiation for correct tissue development and homeostasis. Defects in this balance can lead to developmental defects or tumor formation. In recent years, mRNA splicing has emerged as an important mechanism regulating cell fate decisions. Here we address the role of the evolutionarily conserved splicing co-factor Barricade (Barc)/Tat-SF1/CUS2 in *Drosophila* neural stem cell (neuroblast) lineage formation. We show that Barc is required for the generation of neurons during *Drosophila* brain development by ensuring correct neural progenitor proliferation and differentiation. Barc associates with components of the U2 small nuclear ribonucleoprotein (snRNP) complex, and its depletion causes alternative splicing in the form of intron retention in a subset of genes. Using bioinformatics analysis and a cell culture-based splicing assay, we found that Barc-dependent introns share three major traits: they are short, GC rich and have weak 3′ splice sites. Our results show that Barc, together with the U2 snRNP complex, plays an important role in regulating neural stem cell lineage progression during brain development and facilitates correct splicing of a subset of introns.

KEY WORDS: *Drosophila*, Splicing, Intron retention, Brain development, Barricade, Cell cycle

INTRODUCTION

Stem cells have the unique ability to generate differentiating daughter cells while maintaining their stem cell fate. This process needs to be tightly balanced for correct tissue development (Morrison and Kimble, 2006; Shenghui et al., 2009; Weissman, 2000). During brain development, failure to limit stem cell proliferation or to establish a differentiated state can result in ectopic stem cells that proliferate unrestrictedly and cause tumorigenic overgrowth, as in the case of pediatric brain tumors (Eberhart, 2007; Hemmati et al., 2003; Wang and Wechsler-Reya, 2014). By contrast, premature progenitor cell differentiation or cell cycle exit can result in cortical malformations (Bizzotto and Francis, 2015; Colasante et al., 2015; Mao et al., 2015; Pilaz et al., 2016; Silver et al., 2010). Thus, tight regulation of stem cell self-renewal and differentiation is crucial for tissue development and the prevention of pathological states.

The *Drosophila* larval brain harbors neural stem cells called neuroblasts (NBs) that divide asymmetrically into a self-renewing NB and a differentiating daughter cell. Per central brain lobe, there are ∼100 type I NBs [expressing the markers Miranda (Mira), Deadpan (Dpn) and Asense (Ase)], and eight type II NBs (expressing Mira and Dpn but not Ase). Upon asymmetric cell division, type I NBs produce a ganglion mother cell [GMC; expressing Ase and Prospero (Pros)], which divides into two neurons or glia cells (Doe, 2008; Homem and Knoblich, 2012; Knoblich, 2008; Reichert, 2011).

Type II NBs produce intermediate neural progenitors (INPs), which mature and undergo four to six asymmetric cell divisions, generating a new INP and a GMC each time (Bello et al., 2008; Boone and Doe, 2008; Bowman et al., 2008). While all INPs express Mira, the immature INPs are initially Ase$^-$ Dpn$^-$, but as they mature they re-express first Ase, then Dpn (Fig. 1A) (Bayraktar et al., 2010; Bowman et al., 2008). As they contain a transient amplifying population of INPs, type II NBs generate more than twice as many progeny as a type I NB (Bello et al., 2008) and they are often compared to mammalian neural stem cells (Homem and Knoblich, 2012).

It has been demonstrated that INPs pass through different windows of competence as they age. This temporal patterning is achieved by sequential expression of the transcription factors Dichaete, Grainy head and Eyeless, and contributes to increasing the neural diversity in the brain (Bayraktar and Doe, 2013).

Limited cell migration and distinctive marker combinations present in NBs and their progeny make the *Drosophila* larval brain a good system with which to study stem cell self-renewal and differentiation (Dumstrei et al., 2003; Kang and Reichert, 2015; Reichert, 2011; Spindler and Hartenstein, 2010; Weng and Lee, 2011; Weng et al., 2010). Several studies have identified factors and mechanisms that regulate the self-renewal and differentiation of NBs and their progeny (Homem et al., 2015; Kang and Reichert, 2015).

In a genome-wide RNAi screen for regulators of NB self-renewal, we identified a lineage regulator, *barricade* (*barc*) (Neumüller et al., 2011). Knockdown of *barc* induced a differentiation block resulting in an accumulation of INPs, a phenotype distinct from those caused by knockdown of other INP regulators (Neumüller et al., 2011). Barc is the *Drosophila* homolog of mammalian Tat-specific factor 1 (Tat-SF1; HTATSF1) and yeast CUS2. Tat-SF1 was first identified as a co-factor stimulating Tat-directed HIV-1 transcriptional elongation (Zhou and Sharp, 1996) and was later found to be a general transcriptional elongation factor (Chen et al., 2009; Li and Green, 1998; Parada and Roeder, 1999). Consistent with the yeast homolog CUS2, which has a well-characterized role in splicing (Perriman and Ares, 2000, 2007; Perriman et al., 2003; Rodgers et al., 2016; Yan et al., 1998), Tat-SF1 has also been suggested to

[1]Institute of Molecular Biotechnology of the Austrian Academy of Science (IMBA), Dr. Bohr-Gasse 3, 1030 Vienna, Austria. [2]Research Institute of Molecular Pathology (IMP), Campus-Vienna-Biocenter 1, 1030 Vienna, Austria. [3]Biozentrum, University of Basel, Klingelbergstrasse 50, CH-4056 Basel, Switzerland.
*Present address: Commonwealth Scientific and Industrial Research Organisation (CSIRO), Agriculture and Food, Canberra, ACT 2601, Australia. ‡Present address: D-BSSE ETH Zürich, Mattenstrasse 26, CH-4058 Basel, Switzerland.

§Author for correspondence (Juergen.Knoblich@imba.oeaw.ac.at)

J.A.K., 0000-0002-6751-3404

Received 22 March 2017; Accepted 11 September 2017

Development (2017) 144, 3932-3945 doi:10.1242/dev.152199

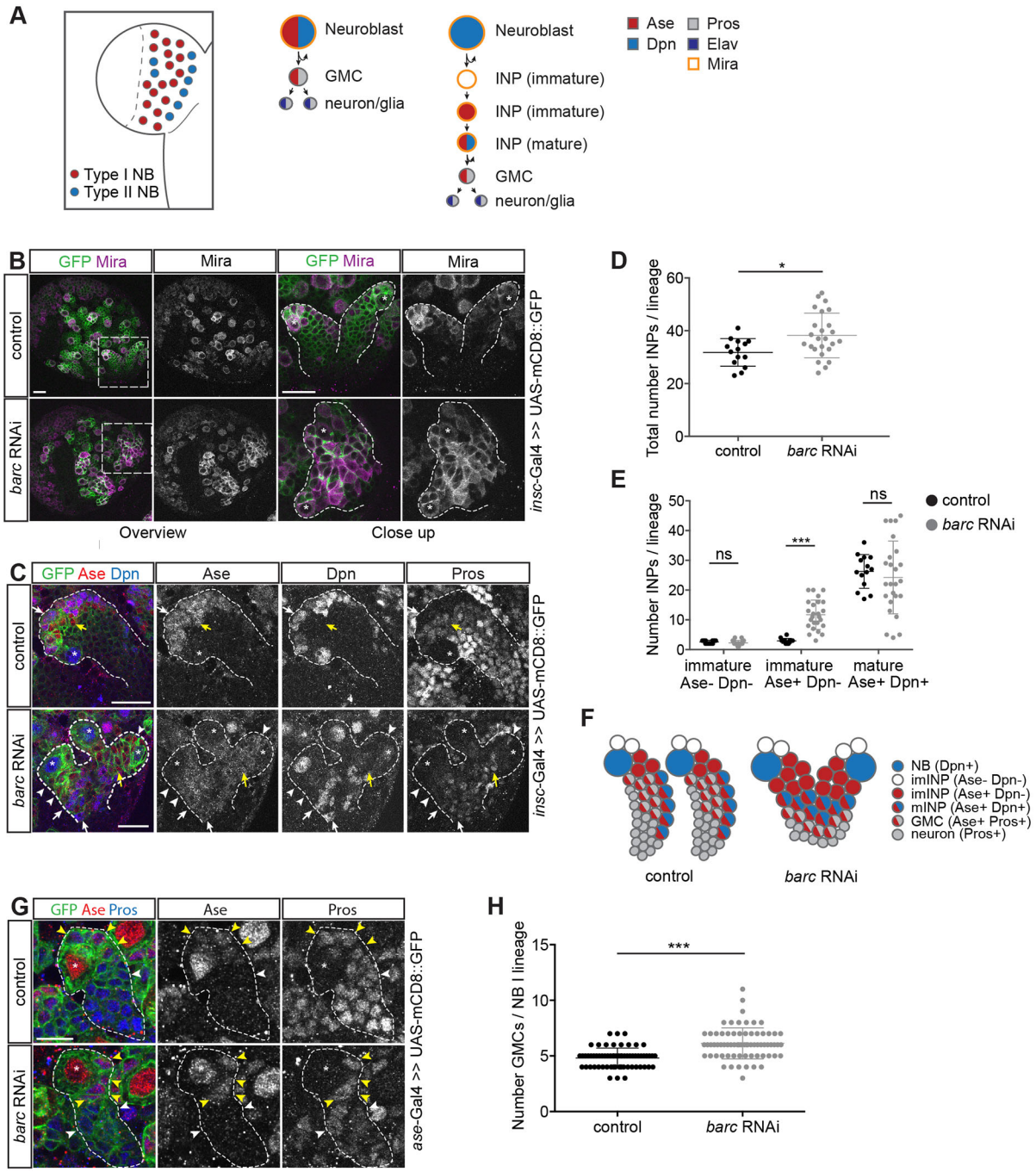

Fig. 1. Knockdown of *barc* increases progenitor cell numbers. (A) Schematic of a *Drosophila* larval central brain lobe with type I and II neuroblast (NB) lineages and expressed markers. (B,C) Representative wild-type and *barc* RNAi type II NB lineages, labeled by coexpressed UAS-mCD8::GFP. RNAi was expressed using *insc*-Gal4. (B) Overview and magnification of type II lineages upon *barc* knockdown. Mira labels progenitor cells. Asterisks, type II NBs. Compared with separated control lineages, *barc* RNAi type II lineages are often close together. (C) *barc* RNAi type II lineages display an accumulation of immature Ase$^+$ Dpn$^-$ Pros$^-$ INPs and fewer GMCs and neurons compared with control. Asterisks, type II NBs; white arrowheads, immature INPs (Ase$^+$ Dpn$^-$ Pros$^-$); white arrows, mature INPs (Ase$^+$ Dpn$^+$ Pros$^-$); yellow arrows, GMCs (Ase$^+$ Dpn$^-$ Pros$^+$). (D) Quantification of total INP numbers per dorsomedial type II lineage. Control: *n*=14 lineages, 3 brains. *barc* RNAi: *n*=25 lineages, 6 brains. (E) Quantification of immature (Ase$^-$ Dpn$^-$ Pros$^-$ and Ase$^+$ Dpn$^-$ Pros$^-$) and mature (Ase$^+$ Dpn$^+$ Pros$^-$) INPs in wild-type and *barc* RNAi type II lineages. Based on the same dataset as in D. (F) Model depicting the altered type II lineage composition upon *barc* knockdown. (G) Type I NB lineages in the central brain. RNAi was expressed using *ase*-Gal4. Asterisks, type I NBs; yellow arrowheads, Ase$^+$ Pros$^+$ GMCs; white arrowheads, neurons (Ase$^-$ Pros$^+$). (H) Quantification of GMC numbers per type I lineage. *barc* knockdown results in increased GMC numbers. Control: *n*=64 lineages, 4 brains. *barc* RNAi: *n*=70 lineages, 4 brains. Quantification based on control and *barc* RNAi expressed using *ase*-Gal4. Data are mean±s.d. Student's *t*-test (D,H). Two-way ANOVA (E). ns, non significant; *P<0.05, ***P<0.001. Scale bars: 20 µm in B,C; 10 µm in G.

play a role in splicing (Fong and Zhou, 2001; Miller et al., 2011, 2009; Yan et al., 1998; Zhou et al., 2002). However, its specific role in this process has not been characterized. In addition, there are no *in vivo* studies of Tat-SF1 in higher eukaryotes, nor are there studies addressing its role in the context of stem cell self-renewal and differentiation.

Development (2017) 144, 3932-3945 doi:10.1242/dev.152199

Here, we employed the *Drosophila* NB system to investigate the role of Barc in neural stem cell differentiation *in vivo*. We show that loss of Barc results in a cell cycle defect in the neural progenitor cells, and in an accumulation of INPs and GMCs at the expense of neurons. We further show that Barc associates with members of the U2 snRNP complex and plays a crucial role to ensure proper and efficient splicing of short, GC-rich introns with weak 3′ splice sites.

RESULTS

barc loss of function causes an accumulation of neural progenitor cells at the expense of neurons

We have previously identified *barc* as a regulator of *Drosophila* neural stem cell lineage progression, and revealed that Barc is a nuclear protein expressed in all cells of type I and II NB lineages (Neumüller et al., 2011). Expression of a UAS-*barc* RNAi construct using *insc*-Gal4 (the *insc*-Gal4>>UAS-mCD8::GFP driver line is used throughout the present study unless otherwise stated), resulted in an accumulation of Mira^{+} INPs in dorsomedial type II NB lineages (Fig. 1B) (Neumüller et al., 2011). Quantification confirmed that the total number of INPs per lineage was increased by 20% upon *barc* RNAi [38.2±2.2 (±s.e.m.) upon *barc* RNAi versus 31.8±1.4 in control] (Fig. 1D).

Analysis of the INP composition showed that, on average, Barc-depleted dorsomedial type II lineages exhibited no difference in Ase^{-} Dpn^{-} immature INP numbers but a 300% increase (11.7±1.3 upon *barc* RNAi versus 2.9±0.2 in control) in immature Ase^{+} Dpn^{-} INP numbers (Fig. 1C,E). No significant difference (24.2±3.3 upon *barc* RNAi versus 26.3±1.5 in control) was observed in mature Ase^{+} Dpn^{+} INP numbers (Fig. 1C,E). There were also fewer GMCs and Pros^{+} neurons in the *barc* RNAi type II lineage clusters (Fig. 1C,F). This suggests that the increase in INP numbers upon Barc depletion may be due to impaired INP maturation and differentiation.

In order to test if the *barc* RNAi type I lineages also displayed an accumulation of progenitor cells we counted GMC numbers. Whereas control type I lineages contained 4.8±0.1 GMCs per lineage, *barc* RNAi resulted in 6.1±0.2 GMCs per lineage upon *ase*-Gal4-mediated *barc* knockdown (Fig. 1G,H). A similar accumulation was observed upon *insc*-Gal4-mediated *barc* knockdown (Fig. S1B). Similarly to the type II lineages, staining for the neuronal markers Pros and Elav showed a decreased neuronal output upon *barc* RNAi (using *ase*-Gal4) (Fig. 1G, Fig. S1A).

To ensure that the observed *barc* RNAi phenotype is specific to the loss of Barc, we overexpressed an RNAi-resistant *barc* coding sequence in the *barc* RNAi background. This rescued both the type II and type I lineage phenotypes (Fig. S2A,C,D; type I rescue not shown) (Neumüller et al., 2011). Taken together, these data suggest that Barc is required for neuronal progenitors to both proliferate and differentiate into neurons.

barc mutant clones confirm immature INP accumulation and underproliferation

To gain more insight into the *barc* loss-of-function phenotype, we generated a *barc* loss-of-function allele using CRISPR. *barc*$^{m4\text{-}2}$ harbors a deletion in exon 2, which causes a frameshift and premature stop (Fig. 2A). As the homozygous mutant is early lethal, we used the MARCM system (Lee and Luo, 1999) to generate homozygous mutant NB clones in a heterozygous mutant background. Similar to the RNAi phenotype, 90-96 h *barc* mutant type II NB clones consisted of Mira^{+} INPs and comparatively few neurons (Fig. 2B,C). In contrast to the control clones, *barc* mutant clones contained many Mira^{+} Ase^{+} Dpn^{-} INPs (Fig. 2B,C). Careful quantification confirmed the accumulation of immature Ase^{+} Dpn^{-} Pros^{-} INPs and revealed a decrease in mature Ase^{+} Dpn^{+} Pros^{-} INPs (Fig. 2E, Fig. S3). Overall there was no difference in total INP numbers (Fig. 2D). Thus, the *barc* mutant clones display a phenotype similar, but not identical, to the *barc* RNAi phenotype. This can be explained by different *barc* depletion efficiency, different timing of the phenotype analysis or fewer analyzed type II clones compared with RNAi depleted type II lineages. Consistent with the *barc* RNAi phenotype, the type I NB clones displayed an increase in GMC numbers (Fig. 2F,G). Quantification revealed a severe decrease in total cell numbers in both type I and II NB lineages, predominantly due to loss of neurons (Fig. 2F,H,I). Overall, key phenotypes were consistent between the *barc* mutant clones and the RNAi phenotype, and further insights were derived from the MARCM clones confirming the underproliferation of the *barc* RNAi phenotype (Fig. 2J,K).

Overexpression of mouse Tat-SF1 rescues the *barc* RNAi phenotype

To test if the Barc function is evolutionarily conserved, we generated a myc-tagged mouse Tat-SF1 transgene and overexpressed it in a *barc* RNAi background. Interestingly, the mammalian homolog also rescued the *barc* RNAi phenotype, indicating that the fly and mammalian homologs indeed have conserved functions (Fig. S2B-D).

barc RNAi alters INP temporal patterning and causes neuroanatomical defects in adult brain morphology

INPs sequentially express the young INP marker Dichaete (D), the middle-age INP marker Grainy head (Grh) and the old INP marker Eyeless (Ey) (Bayraktar and Doe, 2013) (Fig. S4A). As inhibition of *barc* by RNAi affected INP maturation, we tested whether it also affects their temporal patterning. Indeed, INPs appeared stuck at the D^{+} Grh^{-} stage due to maintained D expression but no re-expression of Grh or Ey (Fig. S4B,C). This suggests that Barc is important for both the maturation and temporal patterning of INPs.

INP progeny generated during larval stages contribute strongly to the adult brain structure called the central complex (CCX) (Bayraktar and Doe, 2013; Bayraktar et al., 2010; Izergina et al., 2009; Viktorin et al., 2011). As *barc* RNAi has a strong INP phenotype, we knocked down *barc* using *PntP1*-Gal4, which is expressed in all type II NB lineages in larval brains (Zhu et al., 2011) and in a small subset of type II NB-derived neurons that innervate the CCX in adults (Fig. S5). This resulted in adult brains with neuroanatomical defects in the CCX and a decreased number of type II NB-derived neurons, which localize in the posterior brain region (Fig. S5). Thus, Barc-depleted type II lineages fail to produce sufficient neurons for the correct development of adult brain structures.

Barc-depleted neural progenitor cells display an extended cell cycle with a G2/M delay

The accumulation of progenitors and their increased lifespan could be caused by defects in cell division, differentiation or the cell cycle. Our initial characterization revealed larger type I NBs upon *barc* RNAi (Neumüller et al., 2011), a phenotype consistent with a cell cycle delay (Neufeld et al., 1998). We confirmed this phenotype in type I NBs as well as in Barc-depleted GMCs, type II NBs and INPs (Fig. S6A-D).

To address the effect of *barc* RNAi on cell cycle progression, we quantified the cell cycle length in control and *barc* RNAi conditions

Development (2017) 144, 3932-3945 doi:10.1242/dev.152199

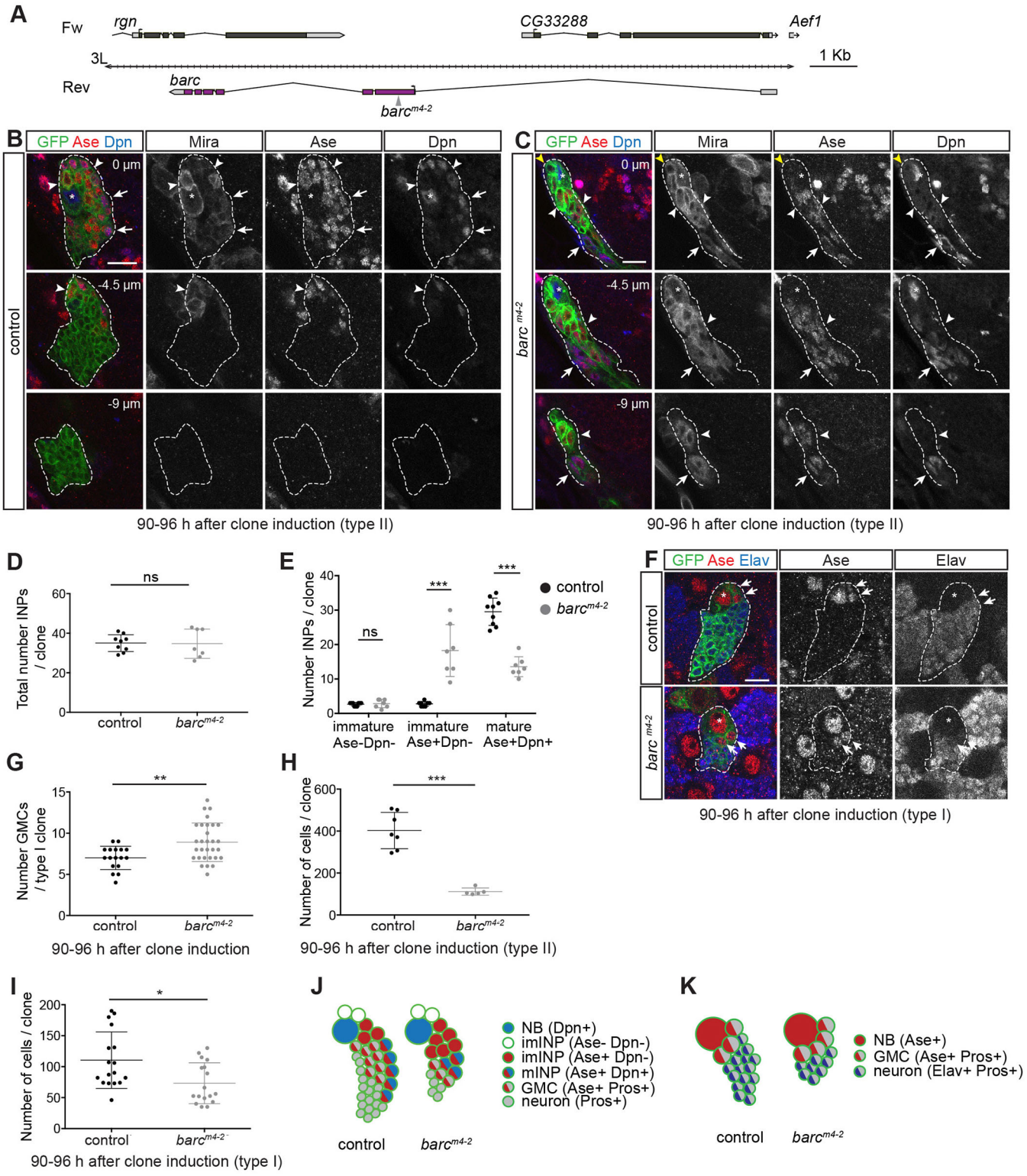

Fig. 2. *barc* mutants confirm GMC and immature INP accumulation at the expense of neurons. (A) The *barc* genomic locus. The *barc*$^{m4-2}$ mutant allele results from a one nucleotide deletion in exon 2, leading to a frameshift and premature stop codons. (B,C) Dorsomedial control (B) and *barc*$^{m4-2}$ mutant (C) type II NB MARCM clones 90-96 h after clone induction. Three separate *z*-planes are included to show the NBs, INPs and neurons. Asterisks, NBs; yellow arrowheads, Mira$^+$ Ase$^-$ Dpn$^-$ INPs; white arrowheads, Mira$^+$ Ase$^+$ Dpn$^-$ INPs; arrows, Mira$^+$ Ase$^+$ Dpn$^+$ INPs. (D) Total INP numbers per control or *barc*$^{m4-2}$ mutant type II NB MARCM clone. Control: *n*=9 clones, 8 brains. *barc*$^{m4-2}$: *n*=7 clones, 6 brains. (E) Quantification of immature (Ase$^-$ Dpn$^-$ Pros$^-$ and Ase$^+$ Dpn$^-$ Pros$^-$) and mature (Ase$^+$ Dpn$^+$ Pros$^-$) INPs in control or *barc*$^{m4-2}$ mutant type II NB MARCM clones. Based on the same dataset as in D. (F) 90-96 h control and *barc*$^{m4-2}$ type I NB MARCM clones. Asterisks, NBs; arrows, GMCs. (G) Quantification of GMC numbers per control or *barc*$^{m4-2}$ mutant type I NB clone. Control: *n*=17 clones, 7 brains. *barc*$^{m4-2}$: *n*=30 clones, 12 brains. (H) Total cell numbers per control or *barc*$^{m4-2}$ mutant type II NB MARCM clone. Control: *n*=7 clones, 7 brains. *barc*$^{m4-2}$: *n*=5 clones, 4 brains. (I) Total cell numbers per control or *barc*$^{m4-2}$ mutant type I NB MARCM clone. Control: *n*=17 clones, 7 brains. *barc*$^{m4-2}$: *n*=17 clones, 6 brains. (J,K) Models depicting the altered type II (J) and type I (K) lineage composition in *barc* mutants. Data are mean±s.d. Student's *t*-test (D,G,H,I). Two-way ANOVA (E). ns, non significant; *P<0.05, **P<0.01, ***P<0.001. Scale bars: 10 µm.

Development (2017) 144, 3932-3945 doi:10.1242/dev.152199

using live cell imaging (Homem et al., 2013). Indeed, Barc-depleted type II NBs (RNAi expressed using *wor*-Gal4, *ase*-Gal80) divided on average 35% (32 min) slower than controls (Fig. 3A,B). Likewise, the INP maturation time (from cell formation to first division) was extended on average by 58% (3 h) upon loss of Barc (Fig. 3C). *barc* knockdown (using *ase*-Gal4) extended the cell cycle of type I NBs on average by 23% (18 min; Fig. 3E,F) and of GMCs by 25% (1 h; Fig. 3G). Thus, loss of Barc extends the cell cycle of all three types of neural progenitor cells (Fig. 3D,H).

Using FACS analysis we assessed the DNA content in INPs and GMCs (as they are more abundant than NBs), which revealed a higher proportion of cells in G2/M phase upon *barc* RNAi (Fig. 3I,J). Consistently, Barc is also required for proper cell cycle progression in S2 cells (Fig. S7A,B) (Andersen and Tapon, 2008). Thus, Barc is necessary for proper cell cycle progression in both neural progenitors and S2 cells.

Barc associates with the U2 snRNP complex

To understand the molecular function of Barc, we analyzed its binding partners using a transgenic HA-tagged Barc protein (Fig. S8A-C). Upon immunoprecipitation of Barc from larval brains and subsequent MS analysis we identified 15 binding partners (Table S1). Using STRING (Szklarczyk et al., 2015) we analyzed the relationships of the interactors (Fig. 4A). Barc strongly interacted with several splicing factors, which are important for both prespliceosome formation and the U2 small nuclear ribonucleoprotein (U2 snRNP) complex, one of several multiprotein complexes that bind to introns during pre-mRNA splicing (Herold et al., 2009; Mount and Salz, 2000; Will and

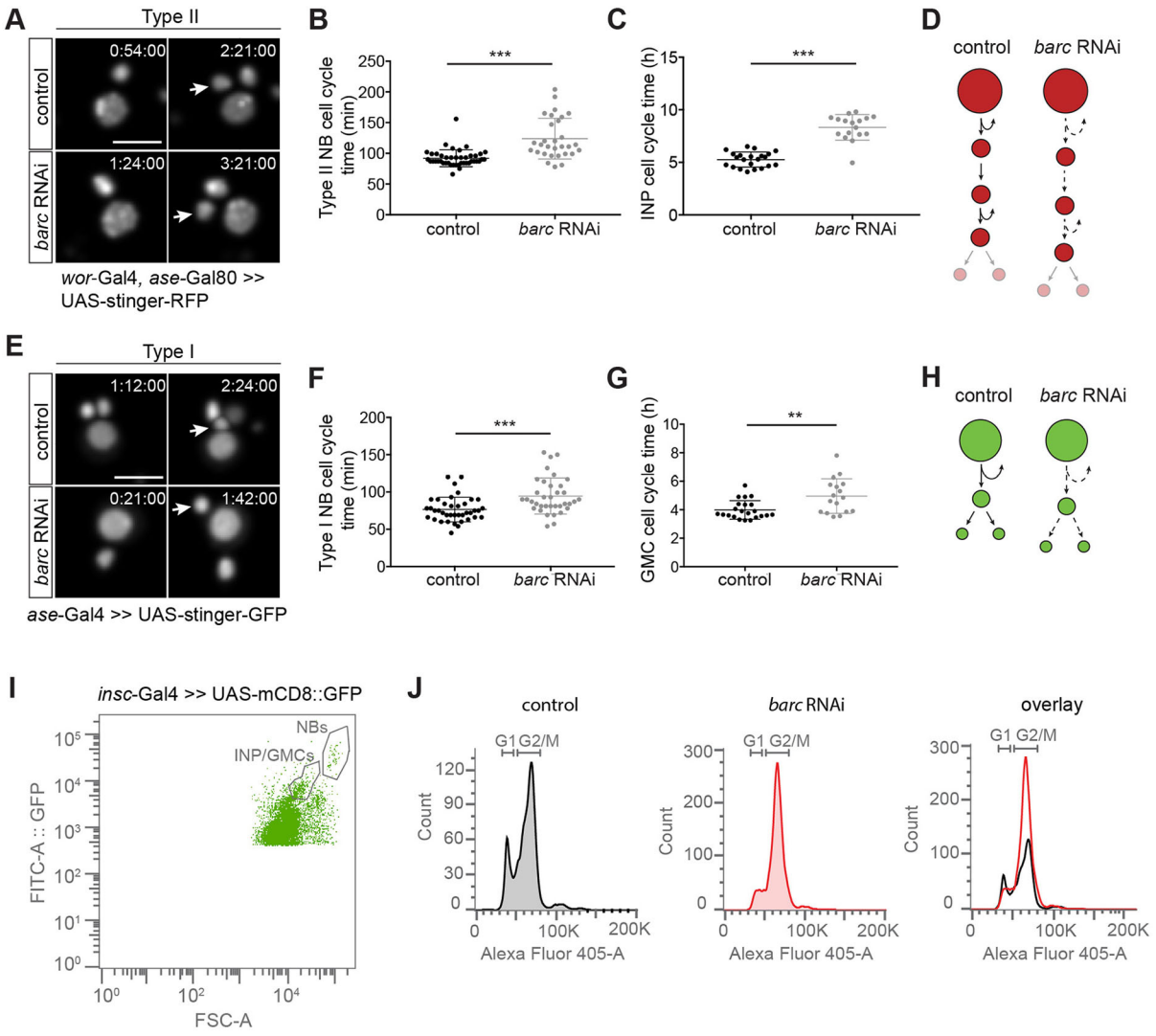

Fig. 3. *barc* loss of function results in increased cell cycle duration with a G2/M phase delay. (A) Frames from live cell imaging movies of control and *barc* RNAi type II NBs and INPs in culture. RNAi was expressed using *wor*-Gal4, *ase*-Gal80. Arrow, newly born INP. Time, h:min:s. (B) Quantification of type II NB cell cycle time. Control: *n*=43 NBs, 4 experiments. *barc* RNAi: *n*=30 NBs, 4 experiments. (C) Quantification of the time between birth and division of the first INP. Control: *n*=22 INPs, 4 experiments. *barc* RNAi: *n*=17 INPs, 4 experiments. (D) Model depicting elongated cell cycles of type II NBs and INPs upon *barc* RNAi. GMC cell cycle was not analyzed. (E) Frames from live cell imaging movies of control and *barc* RNAi type I NBs and GMCs in culture. RNAi was expressed using *ase*-Gal4. Arrow, newly born GMC. (F) Quantification of type I NB cell cycle time. Control: *n*=39 NBs, 4 experiments. *barc* RNAi: *n*=36 NBs, 4 experiments. (G) Quantification of the time between birth and division of the first GMC. Control: *n*=22 GMCs, 3 experiments. *barc* RNAi: *n*=17 GMCs, 3 experiments. (H) Model depicting elongated cell cycles of type I NBs and GMCs upon *barc* RNAi. (I) FACS gating strategy (based on Berger et al., 2012; Eroglu et al., 2014) to analyze the INP/GMC population. (J) Representative graphs of DNA content (Hoechst 33342) analysis of the GMC and INP population in control and *barc* RNAi conditions. Control: 4000 cells recorded. *barc* RNAi: 6500 cells recorded. Experiment was replicated twice. Data are mean±s.d. Student's *t*-test. ***P*<0.01, ****P*<0.001. Scale bars: 10 µm.

Development (2017) 144, 3932-3945 doi:10.1242/dev.152199

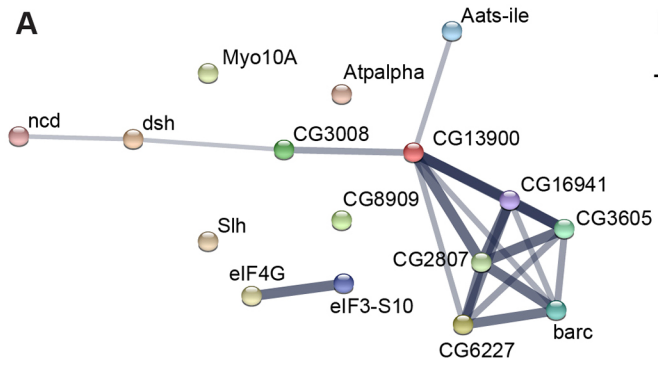

B

pathway ID	pathways	p-value (B-H)	matches
GO:0005686	U2 snRNP	9.35E-06	4
GO:0097525	spliceosomal snRNP complex	1.21E-03	4
GO:0030532	small nuclear ribonucleoprotein complex	2.61E-03	4
GO:0005681	spliceosomal complex	2.64E-03	5
GO:0071013	catalytic step 2 spliceosome	1.22E-02	4
GO:0071011	precatalytic spliceosome	1.91E-02	4

C

Interactor	Mammalian homolog	Function
CG6227	DDX46	prespliceosome
CG2807	SF3B1	U2snRNP
CG16941	SF3A1	U2snRNP
CG13900	SF3B3	U2snRNP
CG3605	SF3B2	U2snRNP

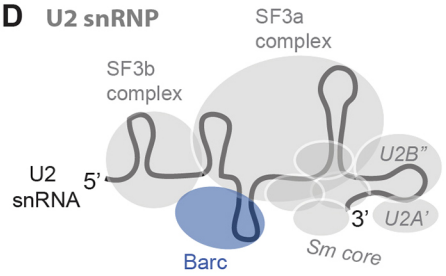

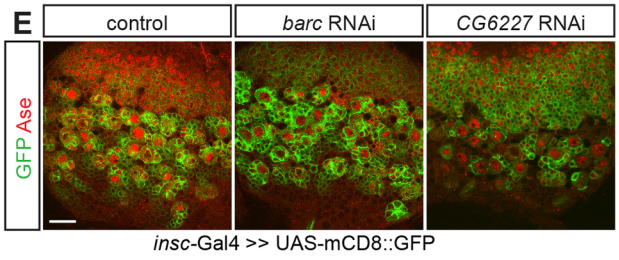

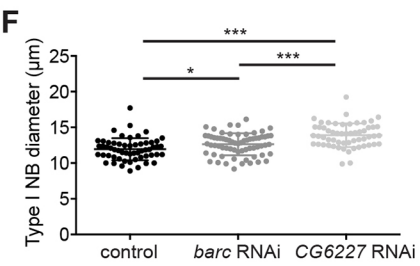

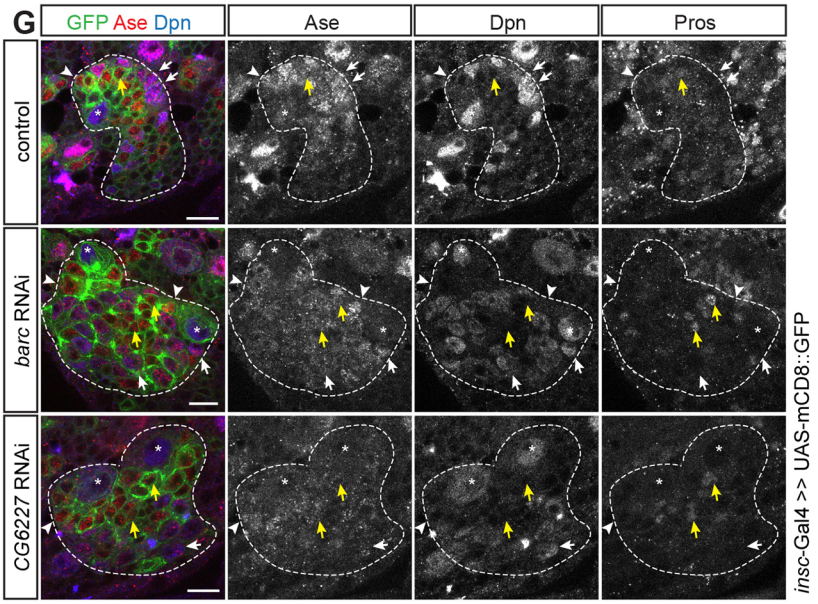

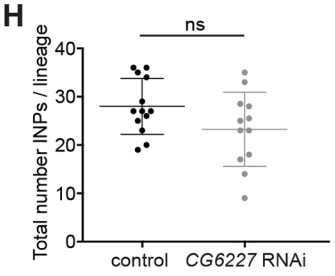

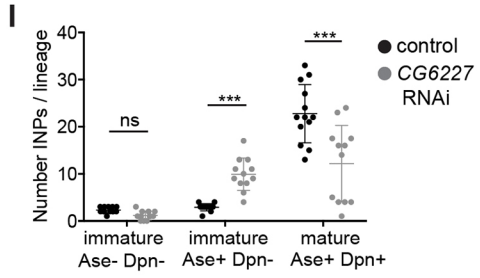

Fig. 4. See next page for legend.

Lührmann, 2011) (Fig. 4B,C). Nuclease treatment of the larval brain extract suggested that most of the interactions between Barc and the splicing factors are dependent on DNA or RNA (Table S1). Additionally, rescue experiments using a transgenic Barc protein with a mutated RNA recognition motif (RRM) suggested that the interaction of Barc with the splicing factors is mediated via RNA (Fig. S9A,B). Thus, Barc associates with U2 snRNP (Fig. 4D) in a nucleic acid-dependent manner, consistent with the described functions of its homologs CUS2 and Tat-SF1 (Fong and Zhou, 2001; Yan et al., 1998; Zhou et al., 2002).

To test whether the interaction of Barc with the U2 snRNP complex is functionally relevant, we depleted four of the most abundant U2 snRNP-related interaction partners. RNAi of the most abundant interactor, *CG6227* (*dPRP5*), a prespliceosome RNA

Development (2017) 144, 3932-3945 doi:10.1242/dev.152199

Fig. 4. Barc interacts with the U2 snRNP complex. (A) Network of significant Barc interactors identified by MS. Nodes represent proteins and edges represent protein-protein associations. The line thickness indicates the strength of the data support (based on known and predicted interactions, text-mining and coexpression information; knowledge of interactions between orthologous proteins in other organisms is transferred). (B) GO term enrichment analysis. *P*-values were adjusted according to the Benjamini-Hochberg (B-H) test correction. (C) Functions and mammalian homologs of the most abundant Barc interactors. (D) Model of the U2 snRNP complex. Barc is placed next to the SF3b and SF3a complexes based on its most abundant interactors. (E) Anterior type I lineages in control, *barc* RNAi- and *CG6227* RNAi-expressing larval (L3) brains. RNAi was expressed using *insc*-Gal4. Coexpressed UAS-mCD8::GFP labels the lineages. Ase labels type I NBs and GMCs. To visualize the GFP expression in the *CG6227* RNAi panel, the GFP level was increased. (F) Quantification of type I NB diameters in control, *barc* RNAi and *CG6227* RNAi brains. Control: *n*=57 NBs, 3 brains. *barc* RNAi: *n*=68 NBs, 3 brains. *CG6227* RNAi: *n*=57 NBs, 3 brains. (G) High-magnification images of control, *barc* RNAi and *CG6227* RNAi type II lineages. RNAi was expressed using *insc*-Gal4. Coexpressed UAS-mCD8::GFP labels the lineages. Asterisks, type II NBs; white arrowheads, immature INPs (Ase^+ Dpn^- $Pros^-$); white arrows, mature INPs (Ase^+ Dpn^+ $Pros^-$); yellow arrows, GMCs (Ase^+ Dpn^- $Pros^+$). (H) Total INP numbers per type II lineage. Control: *n*=13 lineages, 4 brains. *barc* RNAi: *n*=12 lineages, 4 brains. (I) Quantification of immature (Ase^- Dpn^- $Pros^-$ and Ase^+ Dpn^- $Pros^-$) and mature (Ase^+ Dpn^+ $Pros^-$) INPs in wild-type and *CG6227* RNAi type II lineages. Based on the same dataset as in H. Data are mean±s.d. One-way ANOVA (F). Student's *t*-test (H). Two-way ANOVA (I). ns, non significant; **P*<0.05, ****P*<0.001. Scale bars: 20 µm in E; 10 µm in G.

helicase (Mount and Salz, 2000), displayed a phenotype closely related to that of Barc depletion in both the type I and II lineages (Fig. 4E-I), with a tendency to stronger underproliferation (Fig. 4E). We further observed occasional Ase upregulation in the type II NBs (data not shown). As *insc*-Gal4-driven RNAi of the core splicing factors *Sf3b1* (*CG2807*) and *Sf3a1* (*CG16941*) was embryonic lethal, we performed type I NB-specific knockdown (using *ase*-Gal4) of *Sf3b1*, *Sf3a1* and *Sf3b3* (*CG13900*). This also caused underproliferation, but the phenotypes were more severe and resulted in an almost complete loss of type I lineages (Fig. S10). Using a temperature-sensitive *insc*-Gal4 driver, which limits the RNAi expression, we depleted *Sf3b1* in the type II lineage. This resulted in a phenotype similar to that of *barc* RNAi but with the addition of Ase upregulation in the type II NBs (Fig. S11). Altogether, these results suggest that Barc acts in a complex with U2 snRNP and the prespliceosome.

As depletion of various snRNP subunits results in cell cycle defects in the G2/M phase (Andersen and Tapon, 2008; Hofmann et al., 2010; Sundaramoorthy et al., 2014), we tested whether any perturbation of the spliceosome would generate similar phenotypes to those of U2 snRNP depletion. Using the standard *insc*-Gal4 and the temperature-sensitive *insc*-Gal4 drivers, we expressed UAS-RNAi constructs directed against different snRNP core components and observed a gradient of underproliferation phenotypes ranging from relatively normal type II lineages to their complete loss (Fig. S11) (Neumüller et al., 2011). In general, the specific subunit knockdowns displayed phenotypes of different strength, with distinct aspects, but that nevertheless had overlapping features. We conclude that the *barc* RNAi phenotype is related to a general splicing defect phenotype, but still displays distinct subphenotypes.

Barc is important for the proper splicing of a subset of introns

The association of Barc with U2 snRNP complex members suggested a role in pre-mRNA splicing. We performed RNAseq to analyze the effect of *barc* RNAi on splicing both *in vivo* in the abundant type I NBs and in cultured *Drosophila* S2 cells (as both cell types were affected by *barc* RNAi; Fig. 3, Fig. S7).

In total, we identified 63 upregulated and 36 downregulated genes in the type I NB dataset and 296 upregulated and 274 downregulated genes in the S2 dataset (for both datasets: FPKM $\geq$10, $P_{adjusted} \leq 0.01$, $\log_2$ fold change $\geq$1). Importantly, *barc* RNAi in both cell types affected the splicing efficiency of a subset of introns, which remained unspliced in the polyadenylated transcripts. This splicing defect, called intron retention, was confirmed by RT-PCR (Fig. 5A,B, Fig. S12) and Sanger sequencing (data not shown), and is in line with previous observations (Brooks et al., 2015).

Using DEXseq (Anders et al., 2012), we identified 509 significantly retained introns in 479 genes in the type I NB dataset, and 1107 significantly retained introns in 936 genes in the S2 dataset [$P_{adjusted} \leq 0.01$, $\log_2$ fold change $\geq$1, abundance/(intron width) $\geq$0.1] (Table S2). Interestingly, in both the NB and S2 cell datasets, most affected genes retained only one intron, and genes affected in both cell types mostly retained the same intron. Comparison of affected genes in the NB and S2 RNAseq datasets showed an overlap of 305 genes (Fig. 5C) with Gene Ontology (GO) terms that were enriched for categories such as cell cycle, mitotic cell cycle process, DNA repair and mRNA processing (Table S3). Thus, Barc is required for efficient splicing of a subset of introns in both NBs and S2 cells.

Barc-sensitive introns are short, GC rich and have weaker splice sites

To understand the specificity of the *barc* loss-of-function splicing defects, we analyzed the characteristics of the 282 introns retained in both NBs and S2 cells. Barc-dependent introns were significantly shorter than control introns: median Barc-dependent intron (retained), 60 nt; median wild-type expressed intron (expressed), 70 nt; median *D. melanogaster* intron (all), 93 nt (Fig. 5D). We also characterized their GC content. Since short *Drosophila* introns (<81 nt) have different characteristics to long introns (≥81 nt) (Mount et al., 1992), we analyzed the retained introns against (1) the introns from all genes expressed in both the cell types and (2) a random subsample of 282 introns with the same length distribution as the retained intron dataset (Fig. S13). The Barc-dependent introns had a significantly higher GC content than the control introns [median Barc-dependent intron (retained), 0.40; median wild-type expressed intron (expressed), 0.36; median short intron (short introns), 0.33] but still lower than the average exon GC content (0.53) (Zhu et al., 2009) (Fig. 5E). Overall, Barc-sensitive introns tend to be short and GC rich.

In addition to GC content and length, splice site strength is another feature that influences splicing outcome (Sakabe and de Souza, 2007; Shepard et al., 2011). We analyzed the 5′ and 3′ splice site motifs in all common, retained introns from the NB and S2 RNAseq datasets and compared them with the same controls used for the GC content analysis. The Barc-sensitive introns had 5′ and 3′ splice site motifs [including the polypyrimidine tract (PPT)] deviating both from known splice site consensus sequences (Lim and Burge, 2001; Mount et al., 1992) and from a control splice site motif ($Control^{expressed}$) based on all introns expressed in NBs and S2 cells (Fig. 5F). It was previously demonstrated that short *Drosophila* introns have a weaker PPT (containing fewer pyrimidines) than long introns (Mount et al., 1992), but our retained intron dataset displayed an even weaker PPT ($Control^{short}$ versus Retained) as well as a weak intron-exon junction sequence, resulting in a 3′ splice site predicted to be even weaker (Fig. 5F). Thus, Barc-sensitive introns tend to be short, GC rich and have weak splice sites.

Barc-sensitive introns have a weak 3′ splice site

To test whether Barc sensitivity was conveyed by intronic sequence or by the context, we designed a minigene assay to study splicing in

Development (2017) 144, 3932-3945 doi:10.1242/dev.152199

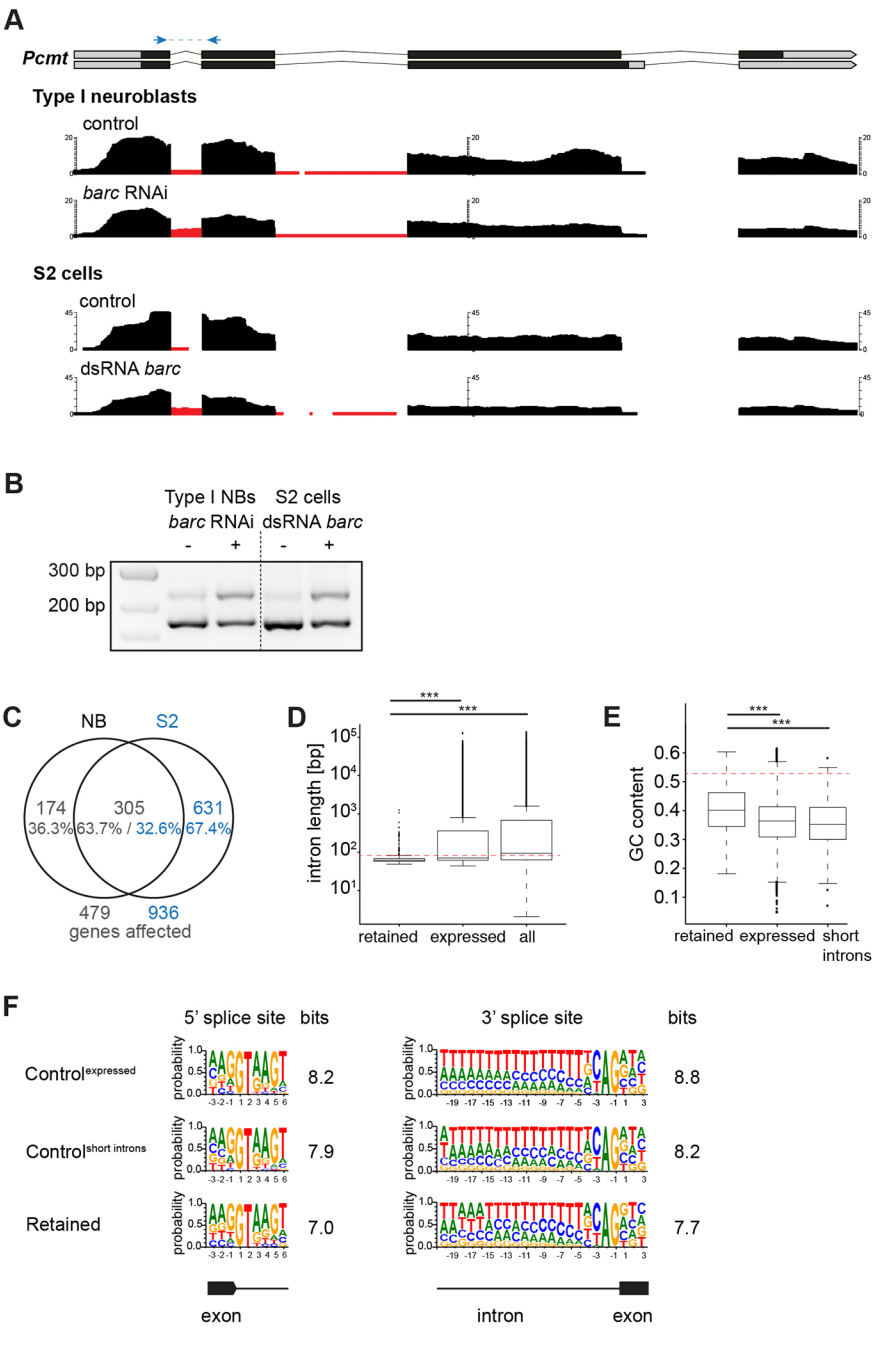

Fig. 5. *barc* knockdown causes intron retention of short, GC-rich introns with weak splice sites. (A) RNA transcripts mapped over the *Pcmt* locus from control and Barc-depleted type I NBs and S2 cells. For each cell type, replicates are merged and normalized. Intronic reads are displayed in red. In both cell types the same intron was retained in the Barc-deficient samples. (B) Intron retention was confirmed by RT-PCR performed on cDNA from control and Barc-depleted type I NBs and S2 cells. The RT-PCR primers span the retained intron and are depicted in blue in A. (C) Genes with retained introns in the NB and S2 datasets. (D) Analysis of intron length for introns retained in Barc-depleted NBs and S2 cells ('retained') and two controls: 'expressed', indicating all expressed introns (n=23,887) in both NBs and S2 cells; and 'all', indicating all *D. melanogaster* introns (n=55,674). Introns below 81 nt (red line) are considered short (Mount et al., 1992). (E) GC content analysis of introns retained in Barc-depleted NB and S2 cells ('retained') and two controls: 'expressed', indicating all expressed introns (n=23,887) in both cell types; and 'short introns', indicating a random subset of 282 introns with the same intron length distribution as the analyzed retained introns. Red line marks average exon GC content (Zhu et al., 2009). (F) Splice site motif analysis using WebLogo (Crooks et al., 2004). The height of each letter is proportional to the frequency of the corresponding base. The most frequent base is at the top. Higher splice site scores (in bits) correspond to stronger splice sites. Analysis was performed on the same datasets as used in E. Wilcoxon rank-sum. ***P<0.001.

S2 cells. We used the *Pcmt* gene, which displayed clear retention of its first, short (<81 nt) and GC-rich (47.5%) intron but not of its second, long intron (≥81 nt) of average (36.9%) GC content. We restricted our analysis to the endogenous sequence between exon 1 and exon 3 (first 282 nt; minigene P_{pcmt}) (Fig. 6A,B). Upon Barc depletion, splicing of the minigene P_{pcmt} recapitulated the previously observed *Pcmt* splicing defects (Fig. 6B′) and thus provided a good system with which to study Barc-dependent splicing. Replacing the first, Barc-sensitive intron with a Barc-independent, short, average GC content (37.5%) intron (intron 11 from *mus205*; minigene P_{mus205}), completely rescued the splicing defect (Fig. 6B,B′, Fig. S14), indicating that *Pcmt* intron 1 splicing is Barc dependent due to the intronic sequence.

This effect could be the result of lower splice site strength in the Barc-sensitive introns. As we identified U2 snRNP as the main interactor of Barc, it is plausible that Barc deficiency acts via U2 snRNP by affecting its stability, conformation or composition. As U2 snRNP binds to the 3′ end of the intron (Will and Lührmann, 2011), we focused on the difference in 3′ splice site strength and tested whether our minigene sequences recapitulated the above 3′ splice site motif analysis. The Barc-sensitive intron (*Pcmt* i-1) had an A-rich 3′ splice site, in contrast to the T-rich 3′ splice site of the Barc-independent intron (*mus205* i-11) (Fig. 6C), and their differential strength was further confirmed by the Berkeley *Drosophila* Genome Project (BDGP) splice site predictor (Reese et al., 1997) (*mus205* i-11, 0.95; whereas no *Pcmt* i-1 3′ splice site could be identified). Given the decreased 3′ splice site strength in Barc-sensitive introns, we tested whether the Barc-dependent splicing was influenced by the strength of the 3′ splice site. Indeed, enhancing the weak 3′ splice site by replacing parts of the *Pcmt* i-1 sequence with 6-48 bp sequence stretches from *mus205* i-11 restored efficient splicing in Barc-depleted cells (minigenes a-e; Fig. 6D).

Development (2017) 144, 3932-3945 doi:10.1242/dev.152199

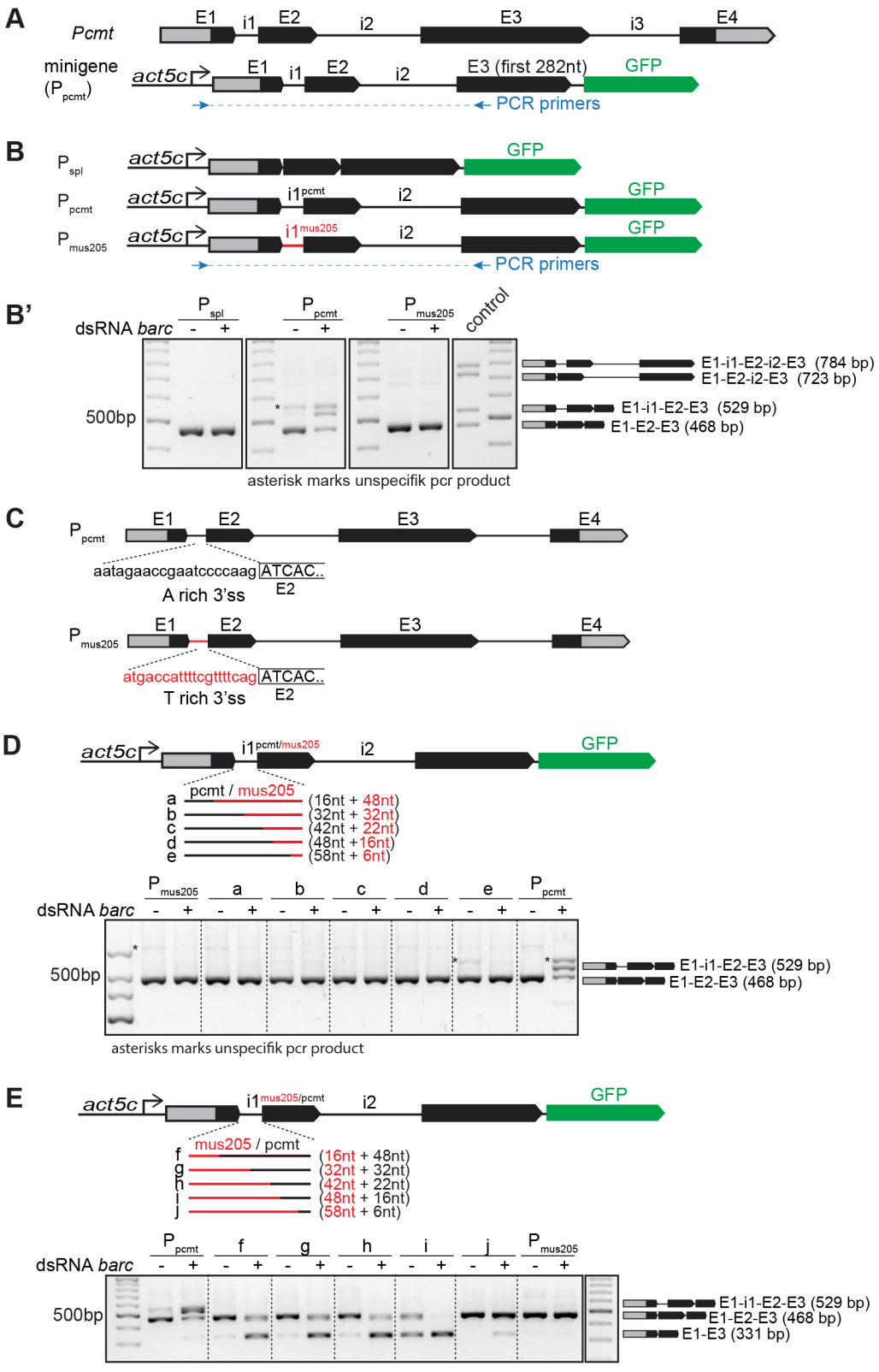

Fig. 6. *Pcmt* minigene assay suggests that Barc facilitates splicing of introns with a weak 3′ splice site. (A) *Pcmt* locus and the *Pcmt* minigene design. i, intron; E, exon. The minigene exon 3 contains only the first 282 nt. (B) Minigene constructs. Construct P_{spl} does not contain any introns and is used as control. Construct P_{pcmt} contains the retained intron (*Pcmt* i-1). In construct P_{mus205}, *Pcmt* i-1 is replaced with a Barc-independent intron of similar size from the *mus205* gene (i-11). Blue arrows (A,B) indicate the location of the RT-PCR primers used in B′,D,E. (B′) Agarose gel of RT-PCR products. RT-PCR was performed on cDNA prepared from the minigene assay in S2 cells. Control lane contains RT-PCR product amplified from minigene vectors. (C) Comparison of the 3′ splice site (3′ss) sequence of *Pcmt* i-1 and *mus205* i-11. (D) Minigene constructs in which parts of the *Pcmt* i-1 3′ splice site and beyond are replaced with corresponding 6-48 nt portions of *mus205* i-11 (minigenes a-e). Agarose gels show minigene RT-PCR products in the presence or absence of Barc. Even the smallest alteration of the *Pcmt* i-1 3′ splice site (minigene e) rescues the Barc-dependent splicing. (E) Minigene constructs in which parts of the *mus205* i-11 3′ splice site and beyond are replaced with corresponding 6-48 nt portions of *Pcmt* i-1 (minigenes f-j). Agarose gels show minigene RT-PCR products in the presence or absence of Barc. Weakening the *mus205* i-11 3′ splice site results in Barc-dependent splicing (f-i). However, instead of intron retention, Barc depletion causes exon skipping.

Conversely, we tested whether a Barc-independent intron (*mus205* i-11 in the P_{mus205} minigene) could become Barc dependent by weakening its 3′ splice site. Replacing parts of the *mus205* i-11 sequence with 6-48 bp sequence stretches from *Pcmt* i-1 (minigenes f-j; Fig. 6E) was indeed sufficient for the splicing of this intron to become Barc dependent. However, instead of resulting in intron retention, we observed Barc-dependent skipping of exon 2 (Fig. 6E), which is another splicing decision influenced by splice site strength or differential GC content between intron and exons (Amit et al., 2012; Ma et al., 2011; Shepard et al., 2011).

As splicing of a terminal intron has been coupled to 3′UTR formation (Kaida, 2016; Rigo and Martinson, 2008), we tested

Development (2017) 144, 3932-3945 doi:10.1242/dev.152199

whether the exon skipping outcome shown in Fig. 6E was due to the original terminal location of *mus205* i-11. We repeated parts of the minigene assay using another Barc-independent *mus205* intron, namely intron 6. Again, minigenes containing hybrid introns between *Pcmt* i-1 and *mus205* i-6 underwent exon skipping upon Barc depletion (Fig. S15). As *mus205* i-6 is a middle intron, and not a terminal intron like i-11, we conclude that the exon skipping outcome shown in Fig. 6E is not due to *mus205* i-11 being a terminal intron. Taken together, these results suggest that a strong 3′ splice site is required for Barc-independent splicing.

We conclude that Barc is a splicing regulator that associates with U2 snRNP and is required for efficient splicing of short, GC-rich introns with weak 3′ splice sites (Fig. 7).

DISCUSSION

Our data show that the *Drosophila* CUS2 and Tat-SF1 (HTATSF1) homolog Barricade (Barc) acts as a cell cycle regulator and is required for neural stem cell lineage specification in the larval brain. Loss of Barc leads to neural progenitor accumulation and insufficient neuronal output. Furthermore, we have shown that Barc is a splicing co-factor, facilitating the splicing of a subset of introns in genes acting in the cell cycle and DNA damage response processes.

Our previous analysis indicated that Barc regulates type II NB lineage progression and that its loss causes INPs to accumulate (Neumüller et al., 2011). In this study, we show that the ectopic INPs predominantly consist of immature Ase^{+} Dpn^{-} INPs, although the exact ratios of immature to mature INPs vary for each lineage. As immature INPs seem to be arrested in G2 phase (Bowman et al., 2008), it is possible that Barc plays a role in timely re-activation of INP proliferation and thereby facilitates their maturation. In recent years, the transcription factors Pointed P1 (PntP1), Earmuff (Erm) and Buttonhead (Btd) have been shown to play important and distinct roles in INP maturation. PntP1 ensures type II identity and INP generation, Erm restricts the developmental potential of INPs, and Btd ensures that the INPs do not undergo premature differentiation (Komori et al., 2014; Weng et al., 2010; Xie et al., 2014; Zhu et al., 2011). Our results suggest that Barc is likewise an INP regulator required for proper INP maturation and temporal patterning. However, it remains to be elucidated if and how these processes are interconnected.

We have also observed that type II lineages contain few GMCs, in contrast to type I lineages, which display an accumulation thereof. However, it is not surprising that the effect of Barc depletion on GMCs might vary between type I and type II NB lineages as they are generated from different cell types in the different lineages, and loss of Barc strongly affects INPs whereas it only mildly affects type I NBs. Therefore, it is more meaningful to compare the effect of Barc depletion in NBs and their immediate progeny cell type (NB I and GMCs, versus NB II and INPs), which in both lineage types are accumulated upon Barc depletion.

An interesting observation is the lack of separation between Barc-depleted type II NB lineages (Fig. 1B,C,F). It is unclear whether the lineages simply lie in close proximity to one another (due to few generated daughter cells pushing them apart), or if the lineages are actually fused together. If the lineages were indeed fused, it could suggest that *barc* is important for the formation and/or maintenance of cortex glia chambers, which surround the NB, GMCs and neurons of individual lineages (Hartenstein, 2011; Pereanu et al., 2005). In the future, it would be interesting to determine whether Barc-depleted type II lineages are fused, and elucidate a potential role of *barc* in cortex glia formation. A better understanding of this process could shed light on the importance of cortex glia for NB lineage development.

We have shown that Barc is in a complex with U2 snRNP and is required for efficient splicing of a subset of introns. Our data are consistent with a model in which splicing of a set of genes is crucial for proper NB lineage progression. In this model, loss of Barc would result in the retention of Barc-sensitive introns in cell cycle, DNA repair and mRNA processing genes. This would result in degraded, truncated or altered proteins, affecting those processes during NB lineage progression.

In this model, two scenarios could explain the *barc* RNAi phenotype. First, Barc could be crucial for adequate splicing of one or a limited number of key target genes. To assess this hypothesis, we picked a few genes, which were highly misspliced upon *barc* knockdown, and performed single-gene rescue experiments. However, none of these genes was able to rescue the *barc* RNAi phenotype when expressed individually (data not shown). Second, the *barc* knockdown phenotype might be caused by a global effect on splicing. This scenario seems particularly plausible since as many as 479 genes were misspliced in the Barc-depleted type I NBs. Although we cannot exclude that, among these inefficiently spliced genes, there are a few that strongly contribute to the phenotype, we currently favor a model whereby the cumulative effect of mild changes in gene expression of many cell cycle, DNA repair and differentiation genes manifest in the observed phenotype.

Although it would be interesting to determine the direct targets of Barc in INPs, the rarity of this cell type meant that we could not collect sufficient material to prepare RNAseq data of good quality. Instead, our RNAseq was performed using the abundant type I NBs,

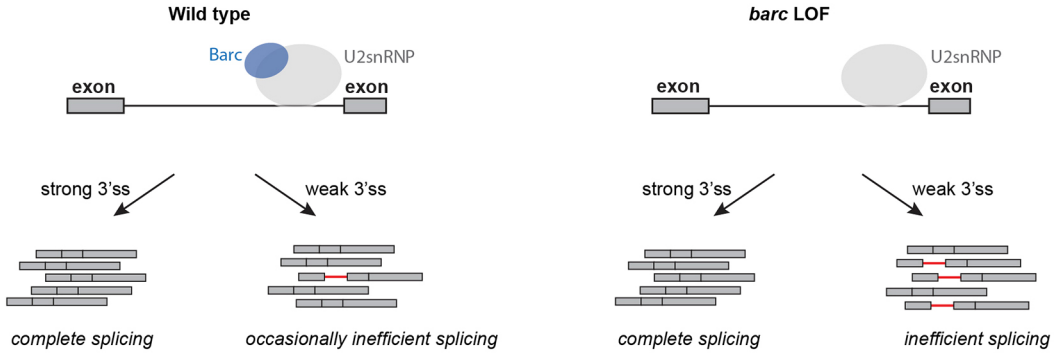

Fig. 7. Model suggesting that loss of Barc disrupts splicing of introns with a suboptimal 3′ splice site. In the presence of Barc, U2 snRNP promotes efficient and complete splicing of introns with both strong and weak 3′ splice sites. Upon Barc depletion, introns with strong 3′ splice sites undergo efficient and complete splicing, whereas introns with weak 3′ splice site are spliced inefficiently, resulting in their retention (red lines).

Development (2017) 144, 3932-3945 doi:10.1242/dev.152199

and although it cannot be employed to identify crucial Barc targets in INPs, it revealed that Barc functions as a splicing co-factor that is important for the proper splicing of a subset of introns in many genes, which suggests that it has a global effect on splicing.

Why are these introns affected in the first place? We have shown that the Barc-sensitive introns in general are short, GC rich and have weak 3′ splice sites, features that impair intron definition by the spliceosome and are likely to make them more sensitive to spliceosomal alterations (Ge and Porse, 2014). An impaired intron-exon distinction by the spliceosome could explain why *barc* RNAi can cause both intron retention and exon skipping, as observed in the minigene assay. This is further supported by previous studies (Ma et al., 2011; Romano et al., 2001; Sakabe and de Souza, 2007; Shepard et al., 2011; Ward and Cooper, 2010; Wickramasinghe et al., 2015; Amit et al., 2012; Galante et al., 2004; Wong et al., 2013).

Interestingly, not only do the retention-prone introns share similar characteristics, but they are also sometimes conserved or located in genes acting in similar processes (e.g. cell cycle, DNA repair, mRNA processing) or in equivalent tissues across different organisms (e.g. the nervous system) (Boutz et al., 2015; Braunschweig et al., 2014; Burns et al., 2002; Dvinge and Bradley, 2015; Galante et al., 2004; Jia et al., 2012; Lareau and Brenner, 2015; Mamon et al., 2013; Sakabe and de Souza, 2007; van der Lelij et al., 2014; Wickramasinghe et al., 2015; Wong et al., 2013). This suggests that retention-prone introns might be biologically significant and could have regulatory functions, an exciting hypothesis in line with previous observations (Boutz et al., 2015; Galante et al., 2004; Ge and Porse, 2014; Wong et al., 2016). Such a biological function of intron retention could be controlled by changes in spliceosome composition due to varying splicing factor levels, which have been shown to vary across cell types and development, and to influence splicing outcomes (Grosso et al., 2008; Papasaikas et al., 2015; Park et al., 2004; Wong et al., 2013).

While mammalian Tat-SF1 has mainly been described to act in transcriptional elongation, our data suggest a stronger functional similarity of Barc with yeast CUS2. Similar to *barc* knockdown, RNAi of *CG6227* (*dPRP5*), the most abundant Barc interactor, also resulted in additional Ase^{+} Dpn^{-} immature INPs, although the total number of INPs was not affected. As RNAi of core splicing factors causes strong underproliferation phenotypes (Fig. S11), it is possible that the discrepancy between the *barc* and *CG6227* RNAi phenotypes is due to CG6227 playing a more universal role in splicing than Barc. Taken together, these results suggest that *barc* and *CG6227* act in the same process in *Drosophila*, a finding consistent with the functions of their yeast homologs (Perriman and Ares, 2000, 2007; Perriman et al., 2003; Rodgers et al., 2016; Yan et al., 1998). Although it is yet to be determined if Barc directly binds RNA (pre-mRNA and/or snRNA), this is plausible as its interaction with U2 snRNP is nucleic acid dependent and its first RNA recognition motif (RRM) is crucial for its function. The same RRM is crucial for mediating the binding of CUS2 and Tat-SF1 to U2 snRNA (Fong and Zhou, 2001; Yan et al., 1998). Taken together, this suggests that Barc might bind U2 snRNA via its RRM1. It would be interesting to test this hypothesis as well as whether Barc depletion affects U2 snRNP conformation or stability.

We have shown that mouse Tat-SF1 is able to rescue the *barc* knockdown phenotype, which suggests functional conservation between the homologs. Given that the function of Tat-SF1 has mostly been studied in a cell culture setting, our results indicate that it would be interesting to test the role of Tat-SF1 in stem cell differentiation in general and in neural cell fate establishment in particular.

MATERIALS AND METHODS

Fly strains, husbandry and clonal analysis

Fly strains are described in the supplementary Materials and Methods. Fly crosses were set up at 25°C, UAS transgenes were expressed at 29°C, and wandering L3 larvae were dissected. For experiments with the temperature-sensitive *tub*-Gal80^{ts}, the crosses were set up and maintained at 18°C for 6 days, followed by 2.5 days at 29°C, then wandering L3 larvae were dissected. For adult stainings, females were dissected at 4-6 days post eclosion. MARCM clones were generated using *elav*-Gal4 (C155), the FLP/FRT system (Lee and Luo, 1999), FRT2A and *barc*$^{m4-2}$ (this study). Larvae were heat shocked for 1 h at 37°C and dissected as wandering L3 larvae (90-96 h post heat shock).

Y287D mutagenesis

The QuikChange Lightning Site-directed Mutagenesis Kit (Agilent Technologies) and primers (Table S4) were used to generate the Y287D substitution in pUASt-*barc*$^{RNAi\text{-}resistant}$ (Neumüller et al., 2011), resulting in pUASt-*barc*$^{RNAiRes\text{-}Y287D}$.

Generation of *barc* shmiR

The *barc*-targeting short hairpin, artificial miRNA (shmiR; Haley et al., 2008) was designed according to Berger et al. (2012). The oligos (Table S4) were annealed and cloned into pValium20 according to the Transgenic RNAi Project protocol (Ni et al., 2011).

Generation of *barc*$^{m4-2}$ mutant

The *barc* mutant was generated using CRISPR/Cas9 in FRT2A flies (BL1997) as described previously (Gokcezade et al., 2014). The gRNA used was 5′-GGCGTTGATGAAGATGTTGA-3′.

The predicted *barc*$^{m4-2}$ peptide (amino acid sequence: MSDEGGCKSEQLEKSEEAEEKKGDAEGQEAKAPILNPISVPEVDDKPTENKPQSDNHADKTDETPSQDFAAYEEHMTYGADGGAIYTDPSTKQKYKWCATGNNWQPLGVDEDVMDRLKIPTKTSTTSGVPNPNSGCQKNRKLKRSTTSGMTSKRSGCPSTRTLARKGFAVWMSMASALTPTRMASSSFGMQPRVLGSPRSMMISWLATK) contains no new domains or repeats, as determined using the InterPro tool (https://www.ebi.ac.uk/interpro/), although the secondary structure might consist of two new alpha helices at the C-terminal end of the peptide, as predicted with the PSIPRED tool (http://bioinf.cs.ucl.ac.uk/psipred/).

Antibodies and immunohistochemistry

Antibodies are listed in the supplementary Materials and Methods. Larval stainings were performed according to Eroglu et al. (2014) and adult stainings according to Jiang and Reichert (2012). Details are provided in the supplementary Materials and Methods. Confocal images were acquired on a Zeiss LSM780 or LSM510 or a Leica TSC-SP5 microscope.

Brain dissociation, primary cell culture and live cell imaging

Primary cultures from larval brains were prepared as described (Homem et al., 2014). Live cell imaging was performed according to Homem et al. (2013). For details, see the supplementary Materials and Methods.

Image processing and statistics

Images were processed using Fiji software (fiji.sc) by adjusting brightness and contrast through the minimum and maximum levels. Unless otherwise stated, all images within an experiment were processed in the same way.

Unpaired two-tailed Student's *t*-test, ANOVA or Wilcoxon rank-sum were used for statistical analysis. $P<0.05$ was considered significant. Scatter dot plots display the mean with s.d. Box plots display the median, the first to the third quartile (the box) and 1.5× the interquartile range (the whiskers). Sample sizes were estimated based on previous experience.

DNA content analysis

Larval brains were dissected, dissociated enzymatically as previously described (Berger et al., 2012) and incubated with Hoechst 33342 (1:1000, Thermo Fisher Scientific) for 45-60 min at room temperature.

Development (2017) 144, 3932-3945 doi:10.1242/dev.152199

dsRNA-treated S2 cells were harvested on day 7, pelleted, washed in PBS and fixed in cold 70% ethanol at least overnight at 4°C. The next day, the fixed cells were washed in PBS and resuspended in PBS with 200 µg/ml RNase A (Thermo Fisher Scientific) and 40 µg/ml propidium iodide (PI) (Thermo Fisher Scientific, P1304MP) and incubated for 1 h at room temperature. The samples were analyzed using FACS (Aria III or LSRFortessa, BD Biosciences), and the data plots were created using FlowJo software.

Immunoprecipitation and mass spectrometry (MS) analysis

Details are provided in the supplementary Materials and Methods. Briefly, L3 brains were homogenized and lysed in lysis buffer [50 mM Tris-HCl pH 8, 100 mM NaCl, 10% glycerol, 0.5% Triton X-100, 1 mM DTT, 1 mM PMSF, 1× Complete EDTA-free protease inhibitor cocktail (Roche)], cleared by centrifugation, snap frozen and stored at −80°C. Thawed lysates were precleared and incubated overnight at 4°C with mouse anti-HA antibody or peptide block (10×). The immunocomplexes were precipitated using Protein G PLUS-agarose beads (Santa Cruz Biotechnology, sc-2002), washed, and eluted by boiling in 2× Laemmli buffer. The proteins were run on 4-12% gradient Bis-Tris gels (NuPAGE, Invitrogen) and subjected to western blotting or a modified version of the Blum silver staining protocol. Nuclease digestion was performed using benzonase (0.1 U/µl, Novagen) before the preclearing.

Protein bands visualized with silver staining were cut out from the gel and processed for MS using in-gel trypsin digest. NanoLC-MS analysis was performed according to Köcher et al. (2012) with slight modifications.

Cutoffs determining significant interactors: minimum ten peptides recovered and minimum 10-fold enrichment over control. Functional groupings and relationships were determined using STRING (Szklarczyk et al., 2015). GO term enrichment was analyzed using Flymine (Lyne et al., 2007).

Western blotting

After SDS-PAGE, the proteins were transferred to nitrocellulose membranes (Hybond ECL, GE Healthcare), blocked with 5% milk solution and incubated overnight at 4°C with rabbit anti-Barc (1:200) (Neumüller et al., 2011), followed by secondary antibody (ECL HRP-conjugated whole antibodies, GE Healthcare) and detected using Pierce ECL Plus (Thermo Scientific).

FACS, library preparation and RNA sequencing

NB sample preparation and FACS analysis and sorting were performed according to Berger et al. (2012).

For RNAseq, L3 brains were used from UAS-*dcr2*; *ase*-Gal4, UAS-mCD8::GFP crossed to control (VDRC, TID60100) or *barc* RNAi (VDRC, TID107013). Type I NBs were collected into TRIzol LS (Invitrogen) and stored at −80°C until enough material was collected. Two biological replicates per genotype were collected and sequenced.

mCherry or *barc* dsRNA-treated S2 cells were collected after 7 days. RNA isolation was carried out using TRIzol. Samples were collected and sequenced from two independent experimental runs, each from two wells (n=2 experiments, 4 wells).

Preparation of mRNA and cDNA for RNAseq was performed as described (Harzer et al., 2013) with slight modifications. Libraries were prepared using the Illumina KAPA Library Preparation Kit or Illumina NEB Ultra Kit. The samples were UDGase treated and subjected to strand-specific paired-end sequencing. See the supplementary Materials and Methods for details.

Computational transcriptome analysis

Differential expression analysis was performed according to Berger et al. (2012). Intron retention was determined using DEXseq (Anders et al., 2012) as described in the supplementary Materials and Methods. GC content was extracted with bedtools (Quinlan and Hall, 2010). Logos and entropy calculation were performed with WebLogo (Crooks et al., 2004). The GO term analysis was performed using Flymine (Lyne et al., 2007).

Tissue culture

S2 cells were cultured in Schneider's *Drosophila* Medium (Life Technologies) supplemented with 10% FBS (Gibco). dsRNA was generated using MEGAscript T7 (Ambion), using the primers listed in Table S4. Transfections were performed using Effectene Transfection Reagent (Qiagen) according to Zhou et al. (2013) with slight modifications.

Gene knockdown and minigene transfection experiments were performed as described (Malone et al., 2014) with slight modifications (see the supplementary Materials and Methods). Minigene sequences are provided in Table S4.

RNA isolation, cDNA synthesis and RT-PCR

RNA was isolated using TRIzol, subjected to DNA digestion (TURBO DNA-free Kit, Ambion) and first-strand cDNA synthesis with random primers (Invitrogen) or oligo(dT) primers (Invitrogen) according to the SuperScript III reverse transcriptase (Invitrogen) protocol.

RT-PCR was performed using GoTaq Green Master Mix (Promega), Taq DNA polymerase (NEB) or Phusion High-Fidelity DNA polymerase (Thermo Scientific) on a C1000 Touch Thermal Cycler (Bio-Rad). Primers are listed in Table S4.

Acknowledgements

We thank all J.A.K. lab members for discussions and support; Francois Bonnay, Magdalena Renner and Martin Breuss for comments on the manuscript; Joseph Gokcezade and Elke Kleiner for assistance; the IMP/IMBA Biooptics Facility for FACS, imaging and image analysis assistance; Thomas Lendl for MARCM clone counting assistance; the IMP/IMBA Protein Chemistry Facility for MS assistance; the Vienna Biocenter Core Facilities (VBCF) Next Generation Sequencing Unit for next generation sequencing assistance; and J. Pielage, the Bloomington *Drosophila* Stock Center, the Vienna *Drosophila* Resource Center (VDRC) and the Developmental Studies Hybridoma Bank for reagents.

Competing interests

The authors declare no competing or financial interests.

Author contributions

Conceptualization: M.K.A., V.R., J.A.K.; Methodology: M.K.A., V.R., P.D.; Software: T.R.B.; Validation: M.K.A.; Formal analysis: M.K.A., T.R.B.; Investigation: M.K.A., V.S., Y.J., S.W.; Resources: M.K.A., T.R.B., V.R., P.D.; Data curation: T.R.B.; Writing - original draft: M.K.A.; Writing - review & editing: V.R., J.A.K.; Visualization: M.K.A.; Supervision: H.R., J.A.K.; Project administration: J.A.K.; Funding acquisition: H.R., J.A.K.

Funding

Work in the J.A.K. laboratory is supported by the Austrian Academy of Sciences, the Austrian Science Fund (Z_153_B09), and an advanced grant from the European Research Council (ERC) (250342 NeuroSyStem MiniBrain). S.W. is supported by a Boehringer Ingelheim Fonds PhD fellowship. Work in the H.R. laboratory is supported by the Swiss National Science Foundation (Schweizerischer Nationalfonds zur Förderung der Wissenschaftlichen Forschung) (NFP63 'Stem Cells and Regenerative Medicine').

Data availability

The RNAseq data are available at the NCBI Gene Expression Omnibus through series accession number GSE96549. The mass spectrometry data have been deposited to the ProteomeXchange Consortium via the PRIDE partner repository with the dataset identifier PXD006068.

Supplementary information

Supplementary information available online at
http://dev.biologists.org/lookup/doi/10.1242/dev.152199.supplemental

References

Amit, M., Donyo, M., Hollander, D., Goren, A., Kim, E., Gelfman, S., Lev-Maor, G., Burstein, D., Schwartz, S., Postolsky, B. et al. (2012). Differential GC content between exons and introns establishes distinct strategies of splice-site recognition. *Cell Rep.* **1**, 543-556.

Anders, S., Reyes, A. and Huber, W. (2012). Detecting differential usage of exons from RNA-seq data. *Genome Res.* **22**, 2008-2017.

Andersen, D. S. and Tapon, N. (2008). Drosophila MFAP1 is required for pre-mRNA processing and G2/M progression. *J. Biol. Chem.* **283**, 31256-31267.

Bayraktar, O. A. and Doe, C. Q. (2013). Combinatorial temporal patterning in progenitors expands neural diversity. *Nature* **498**, 449-455.

Bayraktar, O. A., Boone, J. Q., Drummond, M. L. and Doe, C. Q. (2010). Drosophila type II neuroblast lineages keep Prospero levels low to generate large clones that contribute to the adult brain central complex. *Neural Dev.* **5**, 26.

Bello, B. C., Izergina, N., Caussinus, E. and Reichert, H. (2008). Amplification of neural stem cell proliferation by intermediate progenitor cells in Drosophila brain development. *Neural Dev.* **3**, 5.
Berger, C., Harzer, H., Burkard, T. R., Steinmann, J., van der Horst, S., Laurenson, A.-S., Novatchkova, M., Reichert, H. and Knoblich, J. A. (2012). FACS purification and transcriptome analysis of drosophila neural stem cells reveals a role for Klumpfuss in self-renewal. *Cell Rep.* **2**, 407-418.
Bizzotto, S. and Francis, F. (2015). Morphological and functional aspects of progenitors perturbed in cortical malformations. *Front. Cell. Neurosci.* **9**, 30.
Boone, J. Q. and Doe, C. Q. (2008). Identification of Drosophila type II neuroblast lineages containing transit amplifying ganglion mother cells. *Dev. Neurobiol.* **68**, 1185-1195.
Boutz, P. L., Bhutkar, A. and Sharp, P. A. (2015). Detained introns are a novel, widespread class of post-transcriptionally spliced introns. *Genes Dev.* **29**, 63-80.
Bowman, S. K., Rolland, V., Betschinger, J., Kinsey, K. A., Emery, G. and Knoblich, J. A. (2008). The tumor suppressors Brat and Numb regulate transit-amplifying neuroblast lineages in Drosophila. *Dev. Cell* **14**, 535-546.
Braunschweig, U., Barbosa-Morais, N. L., Pan, Q., Nachman, E. N., Alipanahi, B., Gonatopoulos-Pournatzis, T., Frey, B., Irimia, M. and Blencowe, B. J. (2014). Widespread intron retention in mammals functionally tunes transcriptomes. *Genome Res.* **24**, 1774-1786.
Brooks, A. N., Duff, M. O., May, G., Yang, L., Bolisetty, M., Landolin, J., Wan, K., Sandler, J., Booth, B. W., Celniker, S. E. et al. (2015). Regulation of alternative splicing in Drosophilaby 56 RNA binding proteins. *Genome Res.* **25**, 1771-1780.
Burns, C. G., Ohi, R., Mehta, S., O'Toole, E. T., Winey, M., Clark, T. A., Sugnet, C. W., Ares, M. and Gould, K. L. (2002). Removal of a single alpha-tubulin gene intron suppresses cell cycle arrest phenotypes of splicing factor mutations in Saccharomyces cerevisiae. *Mol. Cell. Biol.* **22**, 801-815.
Chen, Y., Yamaguchi, Y., Tsugeno, Y., Yamamoto, J., Yamada, T., Nakamura, M., Hisatake, K. and Handa, H. (2009). DSIF, the Paf1 complex, and Tat-SF1 have nonredundant, cooperative roles in RNA polymerase II elongation. *Genes Dev.* **23**, 2765-2777.
Colasante, G., Simonet, J. C., Calogero, R., Crispi, S., Sessa, A., Cho, G., Golden, J. A. and Broccoli, V. (2015). ARX regulates cortical intermediate progenitor cell expansion and upper layer neuron formation through repression of Cdkn1c. *Cereb. Cortex* **25**, 322-335.
Crooks, G. E., Hon, G., Chandonia, J.-M. and Brenner, S. E. (2004). WebLogo: a sequence logo generator. *Genome Res.* **14**, 1188-1190.
Doe, C. Q. (2008). Neural stem cells: balancing self-renewal with differentiation. *Development* **135**, 1575-1587.
Dumstrei, K., Wang, F., Nassif, C. and Hartenstein, V. (2003). Early development of the Drosophila brain: V. Pattern of postembryonic neuronal lineages expressing DE-cadherin. *J. Comp. Neurol.* **455**, 451-462.
Dvinge, H. and Bradley, R. K. (2015). Widespread intron retention diversifies most cancer transcriptomes. *Genome Med.* **7**, 45.
Eberhart, C. G. (2007). In search of the medulloblast: neural stem cells and embryonal brain tumors. *Neurosurg. Clin. N. Am.* **18**, 59-69.
Eroglu, E., Burkard, T. R., Jiang, Y., Saini, N., Homem, C. C. F. Reichert, H. and Knoblich, J. A. (2014). SWI/SNF complex prevents lineage reversion and induces temporal patterning in neural stem cells. *Cell* **156**, 1259-1273.
Fong, Y. W. and Zhou, Q. (2001). Stimulatory effect of splicing factors on transcriptional elongation. *Nature* **414**, 929-933.
Galante, P. A. F., Sakabe, N. J., Kirschbaum-Slager, N. and de Souza, S. J. (2004). Detection and evaluation of intron retention events in the human transcriptome. *RNA* **10**, 757-765.
Ge, Y. and Porse, B. T. (2014). The functional consequences of intron retention: alternative splicing coupled to NMD as a regulator of gene expression. *BioEssays* **36**, 236-243.
Gokcezade, J., Sienski, G. and Duchek, P. (2014). Efficient CRISPR/Cas9 plasmids for rapid and versatile genome editing in Drosophila. *G3 (Bethesda)* **4**, 2279-2282.
Grosso, A. R., Gomes, A. Q., Barbosa-Morais, N. L., Caldeira, S., Thorne, N. P., Grech, G., von Lindern, M. and Carmo-Fonseca, M. (2008). Tissue-specific splicing factor gene expression signatures. *Nucleic Acids Res.* **36**, 4823-4832.
Haley, B., Hendrix, D., Trang, V. and Levine, M. (2008). A simplified miRNA-based gene silencing method for *Drosophila melanogaster*. *Dev. Biol.* **321**, 482-490.
Hartenstein, V. (2011). Morphological diversity and development of glia in Drosophila. *Glia* **59**, 1237-1252.
Harzer, H., Berger, C., Conder, R., Schmauss, G. and Knoblich, J. A. (2013). FACS purification of Drosophila larval neuroblasts for next-generation sequencing. *Nat. Protoc.* **8**, 1088-1099.
Hemmati, H. D., Nakano, I., Lazareff, J. A., Masterman-Smith, M., Geschwind, D. H., Bronner-Fraser, M. and Kornblum, H. I. (2003). Cancerous stem cells can arise from pediatric brain tumors. *Proc. Natl. Acad. Sci. USA* **100**, 15178-15183.
Herold, N., Will, C. L., Wolf, E., Kastner, B., Urlaub, H. and Lührmann, R. (2009). Conservation of the protein composition and electron microscopy structure of Drosophila melanogaster and human spliceosomal complexes. *Mol. Cell. Biol.* **29**, 281-301.
Hofmann, J. C., Husedzinovic, A. and Gruss, O. J. (2010). The function of spliceosome components in open mitosis. *Nucleus* **1**, 447-459.
Homem, C. C. F. and Knoblich, J. A. (2012). Drosophila neuroblasts: a model for stem cell biology. *Development* **139**, 4297-4310.
Homem, C. C. F., Reichardt, I., Berger, C., Lendl, T. and Knoblich, J. A. (2013). Long-term live cell imaging and automated 4D analysis of drosophila neuroblast lineages. *PLoS ONE* **8**, e79588.
Homem, C. C. F., Steinmann, V., Burkard, T. R., Jais, A., Esterbauer, H. and Knoblich, J. A. (2014). Ecdysone and mediator change energy metabolism to terminate proliferation in drosophila neural stem cells. *Cell* **158**, 874-888.
Homem, C. C. F., Repic, M. and Knoblich, J. A. (2015). Proliferation control in neural stem and progenitor cells. *Nat. Rev. Neurosci.* **16**, 647-659.
Izergina, N., Balmer, J., Bello, B. and Reichert, H. (2009). Postembryonic development of transit amplifying neuroblast lineages in the Drosophila brain. *Neural Dev.* **4**, 44-13.
Jia, Y., Mu, J. C. and Ackerman, S. L. (2012). Mutation of a U2 snRNA gene causes global disruption of alternative splicing and neurodegeneration. *Cell* **148**, 296-308.
Jiang, Y. and Reichert, H. (2012). Programmed cell death in type II neuroblast lineages is required for central complex development in the Drosophila brain. *Neural Dev.* **7**, 3.
Kaida, D. (2016). The reciprocal regulation between splicing and 3′-end processing. *Wiley Interdiscip. Rev. RNA* **7**, 499-511.
Kang, K. H. and Reichert, H. (2015). Control of neural stem cell self-renewal and differentiation in Drosophila. *Cell Tissue Res.* **359**, 33-45.
Knoblich, J. A. (2008). Mechanisms of asymmetric stem cell division. *Cell* **132**, 583-597.
Köcher, T., Pichler, P., Swart, R. and Mechtler, K. (2012). Analysis of protein mixtures from whole-cell extracts by single-run nanoLC-MS/MS using ultralong gradients. *Nat. Protoc.* **7**, 882-890.
Komori, H., Xiao, Q., Janssens, D. H., Dou, Y. and Lee, C.-Y. (2014). Trithorax maintains the functional heterogeneity of neural stem cells through the transcription factor buttonhead. *eLife* **3**, 183-118.
Lareau, L. F. and Brenner, S. E. (2015). Regulation of splicing factors by alternative splicing and NMD is conserved between kingdoms yet evolutionarily flexible. *Mol. Biol. Evol.* **32**, 1072-1079.
Lee, T. and Luo, L. (1999). Mosaic analysis with a repressible cell marker for studies of gene function in neuronal morphogenesis. *Neuron* **22**, 451-461.
Li, X.-Y. and Green, M. R. (1998). The HIV-1 Tat cellular coactivator Tat-SF1 is a general transcription elongation factor. *Genes Dev.* **12**, 2992-2996.
Lim, L. P. and Burge, C. B. (2001). A computational analysis of sequence features involved in recognition of short introns. *Proc. Natl. Acad. Sci. USA* **98**, 11193-11198.
Lyne, R., Smith, R., Rutherford, K., Wakeling, M., Varley, A., Guillier, F., Janssens, H., Ji, W., Mclaren, P., North, P. et al. (2007). FlyMine: an integrated database for Drosophila and Anopheles genomics. *Genome Biol.* **8**, R129.
Ma, L., Tan, Z., Teng, Y., Hoersch, S. and Horvitz, H. R. (2011). In vivo effects on intron retention and exon skipping by the U2AF large subunit and SF1/BBP in the nematode Caenorhabditis elegans. *RNA* **17**, 2201-2211.
Malone, C. D., Mestdagh, C., Akhtar, J., Kreim, N., Deinhard, P., Sachidanandam, R., Treisman, J. and Roignant, J. Y. (2014). The exon junction complex controls transposable element activity by ensuring faithful splicing of the piwi transcript. *Genes Dev.* **28**, 1786-1799.
Mamon, L. A., Kliver, S. F. and Golubkova, E. V. (2013). Evolutionarily conserved features of the retained intron in alternative transcripts of the *nxf1* (nuclear export factor) genes in different organisms. *OJGen* **3**, 159-170.
Mao, H., Pilaz, L.-J., McMahon, J. J., Golzio, C., Wu, D., Shi, L., Katsanis, N. and Silver, D. L. (2015). Rbm8a haploinsufficiency disrupts embryonic cortical development resulting in microcephaly. *J. Neurosci.* **35**, 7003-7018.
Miller, H. B., Saunders, K. O., Tomaras, G. D. and Garcia-Blanco, M. A. (2009). Tat-SF1 is not required for Tat transactivation but does regulate the relative levels of unspliced and spliced HIV-1 RNAs. *PLoS ONE* **4**, e5710.
Miller, H. B., Robinson, T. J., Gordan, R., Hartemink, A. J. and Garcia-Blanco, M. A. (2011). Identification of Tat-SF1 cellular targets by exon array analysis reveals dual roles in transcription and splicing. *RNA* **17**, 665-674.
Morrison, S. J. and Kimble, J. (2006). Asymmetric and symmetric stem-cell divisions in development and cancer. *Nature* **441**, 1068-1074.
Mount, S. M. and Salz, H. K. (2000). Pre-messenger RNA processing factors in the Drosophila genome. *J. Cell Biol.* **150**, F37-F44.
Mount, S. M., Burks, C., Hertz, G., Stormo, G. D., White, O. and Fields, C. (1992). Splicing signals in Drosophila: intron size, information content, and consensus sequences. *Nucleic Acids Res.* **20**, 4255-4262.
Neufeld, T. P., de la Cruz, A. F. A., Johnston, L. A. and Edgar, B. A. (1998). Coordination of growth and cell division in the Drosophila wing. *Cell* **93**, 1183-1193.
Neumüller, R. A., Richter, C., Fischer, A., Novatchkova, M., Neumüller, K. G. and Knoblich, J. A. (2011). Genome-wide analysis of self-renewal in Drosophila neural stem cells by transgenic RNAi. *Cell Stem Cell* **8**, 580-593.
Ni, J.-Q., Zhou, R., Czech, B., Liu, L.-P., Holderbaum, L., Yang-Zhou, D., Shim, H.-S., Tao, R., Handler, D., Karpowicz, P. et al. (2011). A genome-scale shRNA resource for transgenic RNAi in Drosophila. *Nat. Methods* **8**, 405-407.

Papasaikas, P., Tejedor, J. R., Vigevani, L. and Valcárcel, J. (2015). Functional splicing network reveals extensive regulatory potential of the core spliceosomal machinery. *Mol. Cell* **57**, 7-22.
Parada, C. A. and Roeder, R. G. (1999). A novel RNA polymerase II-containing complex potentiates Tat-enhanced HIV-1 transcription. *EMBO J.* **18**, 3688-3701.
Park, J. W., Parisky, K., Celotto, A. M., Reenan, R. A. and Graveley, B. R. (2004). Identification of alternative splicing regulators by RNA interference in Drosophila. *Proc. Natl. Acad. Sci. USA* **101**, 15974-15979.
Pereanu, W., Shy, D. and Hartenstein, V. (2005). Morphogenesis and proliferation of the larval brain glia in Drosophila. *Dev. Biol.* **283**, 191-203.
Perriman, R. and Ares, M., Jr (2000). ATP can be dispensable for prespliceosome formation in yeast. *Genes Dev.* **14**, 97-107.
Perriman, R. J. and Ares, M. (2007). Rearrangement of competing U2 RNA helices within the spliceosome promotes multiple steps in splicing. *Genes Dev.* **21**, 811-820.
Perriman, R., Barta, I., Voeltz, G. K., Abelson, J. and Ares, M. (2003). ATP requirement for Prp5p function is determined by Cus2p and the structure of U2 small nuclear RNA. *Proc. Natl. Acad. Sci. USA* **100**, 13857-13862.
Pilaz, L.-J., McMahon, J. J., Miller, E. E., Lennox, A. L., Suzuki, A., Salmon, E. and Silver, D. L. (2016). Prolonged mitosis of neural progenitors alters cell fate in the developing brain. *Neuron* **89**, 83-99.
Quinlan, A. R. and Hall, I. M. (2010). BEDTools: a flexible suite of utilities for comparing genomic features. *Bioinformatics* **26**, 841-842.
Reese, M. G., Eeckman, F. H., Kulp, D. and Haussler, D. (1997). Improved splice site detection in Genie. *J. Comput. Biol.* **4**, 311-323.
Reichert, H. (2011). Drosophila neural stem cells: cell cycle control of self-renewal, differentiation, and termination in brain development. *Results Probl. Cell Differ.* **53**, 529-546.
Rigo, F. and Martinson, H. G. (2008). Functional coupling of last-intron splicing and 3′-end processing to transcription in vitro: the poly(A) signal couples to splicing before committing to cleavage. *Mol. Cell. Biol.* **28**, 849-862.
Rodgers, M. L., Tretbar, U. S., Dehaven, A., Alwan, A. A., Luo, G., Mast, H. M. and Hoskins, A. A. (2016). Conformational dynamics of stem II of the U2 snRNA. *RNA* **22**, 225-236.
Romano, M., Marcucci, R. and Baralle, F. E. (2001). Splicing of constitutive upstream introns is essential for the recognition of intra-exonic suboptimal splice sites in the thrombopoietin gene. *Nucleic Acids Res.* **29**, 886-894.
Sakabe, N. J. and de Souza, S. J. (2007). Sequence features responsible for intron retention in human. *BMC Genomics* **8**, 59.
Shenghui, H., Nakada, D. and Morrison, S. J. (2009). Mechanisms of stem cell self-renewal. *Annu. Rev. Cell Dev. Biol.* **25**, 377-406.
Shepard, P. J., Choi, E.-A., Busch, A. and Hertel, K. J. (2011). Efficient internal exon recognition depends on near equal contributions from the 3′ and 5′ splice sites. *Nucleic Acids Res.* **39**, 8928-8937.
Silver, D. L., Watkins-Chow, D. E., Schreck, K. C., Pierfelice, T. J., Larson, D. M., Burnetti, A. J., Liaw, H.-J., Myung, K., Walsh, C. A., Gaiano, N. et al. (2010). The exon junction complex component Magoh controls brain size by regulating neural stem cell division. *Nat. Neurosci.* **13**, 551-558.
Spindler, S. R. and Hartenstein, V. (2010). The Drosophila neural lineages: a model system to study brain development and circuitry. *Dev. Genes Evol.* **220**, 1-10.
Sundaramoorthy, S., Vázquez-Novelle, M. D., Lekomtsev, S., Howell, M. and Petronczki, M. (2014). Functional genomics identifies a requirement of pre-mRNA splicing factors for sister chromatid cohesion. *EMBO J.* **33**, 2623-2642.
Szklarczyk, D., Franceschini, A., Wyder, S., Forslund, K., Heller, D., Huerta-Cepas, J., Simonovic, M., Roth, A., Santos, A., Tsafou, K. P. et al. (2015). STRING v10: protein-protein interaction networks, integrated over the tree of life. *Nucleic Acids Res.* **43**, D447-D452.
van der Lelij, P., Stocsits, R. R., Ladurner, R., Petzold, G., Kreidl, E., Koch, B., Schmitz, J., Neumann, B., Ellenberg, J. and Peters, J.-M. (2014). SNW1 enables sister chromatid cohesion by mediating the splicing of sororin and APC2 pre-mRNAs. *EMBO J.* **33**, 2643-2658.
Viktorin, G., Riebli, N., Popkova, A., Giangrande, A. and Reichert, H. (2011). Multipotent neural stem cells generate glial cells of the central complex through transit amplifying intermediate progenitors in Drosophila brain development. *Dev. Biol.* **356**, 553-565.
Wang, J. and Wechsler-Reya, R. J. (2014). The role of stem cells and progenitors in the genesis of medulloblastoma. *Exp. Neurol.* **260**, 69-73.
Ward, A. J. and Cooper, T. A. (2010). The pathobiology of splicing. *J. Pathol.* **220**, 152-163.
Weissman, I. L. (2000). Stem cells: units of development, units of regeneration, and units in evolution. *Cell* **100**, 157-168.
Weng, M. and Lee, C.-Y. (2011). Keeping neural progenitor cells on a short leash during Drosophila neurogenesis. *Curr. Opin. Neurobiol.* **21**, 36-42.
Weng, M., Golden, K. L. and Lee, C.-Y. (2010). dFezf/Earmuff maintains the restricted developmental potential of intermediate neural progenitors in Drosophila. *Dev. Cell* **18**, 126-135.
Wickramasinghe, V. O., Gonzàlez-Porta, M., Perera, D., Bartolozzi, A. R., Sibley, C. R., Hallegger, M., Ule, J., Marioni, J. C. and Venkitaraman, A. R. (2015). Regulation of constitutive and alternative mRNA splicing across the human transcriptome by PRPF8 is determined by 5′ splice site strength. *Genome Biol.* **16**, 153-121.
Will, C. L. and Lührmann, R. (2011). Spliceosome structure and function. *Cold Spring Harb. Perspect. Biol.* **3**, pii: a003707.
Wong, J. J.-L., Ritchie, W., Ebner, O. A., Selbach, M., Wong, J. W. H., Huang, Y., Gao, D., Pinello, N., Gonzalez, M., Baidya, K. et al. (2013). Orchestrated intron retention regulates normal granulocyte differentiation. *Cell* **154**, 583-595.
Wong, J. J.-L., Au, A. Y. M., Ritchie, W. and Rasko, J. E. J. (2016). Intron retention in mRNA: No longer nonsense. *BioEssays* **38**, 41-49.
Xie, Y., Li, X., Zhang, X., Mei, S., Li, H., Urso, A. and Zhu, S. (2014). The Drosophila Sp8 transcription factor Buttonhead prevents premature differentiation of intermediate neural progenitors. *eLife* **3**, 26-19.
Yan, D., Perriman, R., Igel, H., Howe, K. J., Neville, M. and Ares, M. (1998). CUS2, a yeast homolog of human Tat-SF1, rescues function of misfolded U2 through an unusual RNA recognition motif. *Mol. Cell. Biol.* **18**, 5000-5009.
Zhou, Q. and Sharp, P. A. (1996). Tat-SF1: cofactor for stimulation of transcriptional elongation by HIV-1 Tat. *Science* **274**, 605-610.
Zhou, Z., Licklider, L. J., Gygi, S. P. and Reed, R. (2002). Comprehensive proteomic analysis of the human spliceosome. *Nature* **419**, 182-185.
Zhou, R., Mohr, S., Hannon, G. J. and Perrimon, N. (2013). Inducing RNAi in Drosophila cells by transfection with dsRNA. *Cold Spring Harb. Protoc.* **2013**, 461-463.
Zhu, L., Zhang, Y., Zhang, W., Yang, S., Chen, J.-Q. and Tian, D. (2009). Patterns of exon-intron architecture variation of genes in eukaryotic genomes. *BMC Genomics* **10**, 47-12.
Zhu, S., Barshow, S., Wildonger, J., Jan, L. Y. and Jan, Y.-N. (2011). Ets transcription factor Pointed promotes the generation of intermediate neural progenitors in Drosophila larval brains. *Proc. Natl. Acad. Sci. USA* **108**, 20615-20620.